https://doi.org/10.5194/gmd-2023-50
Preprint. Discussion started: 4 May 2023
© Author(s) 2023. CC BY 4.0 License.

Geoscientific Model Development Discussions

Application of the Multi-Scale Infrastructure for Chemistry and Aerosols version 0 (MUSICAv0) for air quality in Africa

Wenfu Tang[1], Louisa K. Emmons[1], Helen M. Worden[1], Rajesh Kumar[2], Cenlin He[2], Benjamin Gaubert[1], Zhonghua Zheng[3], Simone Tilmes[1], Rebecca R. Buchholz[1], Sara-Eva Martinez-Alonso[1], Claire Granier[4,5], Antonin Soulie[4], Kathryn McKain[5,6], Bruce C. Daube[7], Jeff Peischl[5,8], Chelsea Thompson[8], and Pieternel Levelt[1,9,10]

[1]Atmospheric Chemistry Observations & Modeling Laboratory, National Center for Atmospheric Research, Boulder, CO, USA

[2]Research Applications Laboratory, National Center for Atmospheric Research, Boulder, CO, USA

[3]Department of Earth and Environmental Sciences, The University of Manchester, Manchester M13 9PL, United Kingdom

[4]Laboratoire d'Aérologie, CNRS, Université de Toulouse, Toulouse, France
[5]Cooperative Institute for Research in Environmental Sciences (CIRES), University of Colorado, Boulder, CO, USA
[6]Global Monitoring Laboratory (GML), National Oceanic and Atmospheric Administration, Boulder, CO, USA
[7]Department of Earth and Planetary Sciences, Harvard University, Cambridge, MA, USA
[8]NOAA Chemical Sciences Laboratory, Boulder, CO, USA
[9]Royal Netherlands Meteorological Institute (KNMI), Utrechtseweg 297, 3730 AE De Bilt, the Netherlands
[10]University of Technology Delft, Mekelweg 5, 2628 CD Delft, the Netherlands

Correspondence: Wenfu Tang (wenfut@ucar.edu)

Abstract

The Multi-Scale Infrastructure for Chemistry and Aerosols Version 0 (MUSICAv0) is a new community modeling infrastructure that enables the study of atmospheric composition and chemistry across all relevant scales. We develop a MUSICAv0 grid with Africa refinement (~28 km × 28 km over Africa). We evaluate the MUSICAv0 simulation for 2017 with in situ observations and compare the model results to satellite products over Africa. A simulation from the Weather Research and Forecasting model coupled with Chemistry (WRF-Chem), a regional model that is widely used in Africa studies, is also included in the analyses as a reference. Overall, the performance of MUSICAv0 is comparable to WRF-Chem. Both models underestimate carbon monoxide (CO) compared to in situ observations and satellite CO column retrievals from the Measurements of Pollution in the Troposphere (MOPITT) satellite instrument. MUSICAv0 tends to overestimate ozone (O_3), likely due to overestimated stratosphere-to-troposphere flux of ozone. Both models significantly underestimate fine particulate matter ($PM_{2.5}$) at two surface sites in East Africa. The MUSICAv0 simulation agrees better with aerosol optical depth (AOD) retrievals from the Moderate Resolution Imaging Spectroradiometer (MODIS) and tropospheric nitrogen dioxide

https://doi.org/10.5194/gmd-2023-50
Preprint. Discussion started: 4 May 2023
© Author(s) 2023. CC BY 4.0 License.

Geoscientific Model Development Discussions

(NO_2) column retrievals from the Ozone Monitoring Instrument (OMI) than WRF-Chem. MUSICAv0 has a consistently lower tropospheric formaldehyde (HCHO) column than OMI retrievals. Based on model-satellite discrepancies between MUSICAv0 and WRF-Chem and MOPITT CO, MODIS AOD, and OMI tropospheric NO_2, we find that future field campaign(s) and more in situ observations in an East African region (30°E – 45°E, 5°S – 5°N) could substantially improve the predictive skill of atmospheric chemistry model(s). This suggested focus region exhibits the largest model-in situ observation discrepancies, as well as targets for high population density, land cover variability, and anthropogenic pollution sources.

1. Introduction

As one of the most dramatically changing continents, Africa is experiencing myriad environmental sustainability issues (e.g., Washington et al., 2006; Ziervogel et al., 2014; Boone et al., 2016; Baudoin et al., 2017; Güneralp et al., 2017; Nicholson 2019; Fisher et al., 2021; Kumar et al., 2022). These environmental issues are causing vast losses in lives and in African economies, and are coupled with poverty and under-development (Washington et al., 2006; Fisher et al., 2021). Some of these environmental challenges are particularly severe in Africa compared to many other regions of the world (e.g., famine, droughts, floods, high temperatures, land degradation, and fires; Washington et al., 2006; van der Werf et al., 2017). However, even though Africa is the second largest continent, in land area and population, attention and research on environmental challenges in Africa are very limited, leading to a deficit of knowledge and solutions (e.g., De Longueville et al., 2010). Degraded air quality is an example of a severe environmental challenge with growing importance in Africa (e.g., Liousse et al., 2014; Thompson et al., 2014; Heft-Neal et al., 2018; Fisher et al., 2021; Vohra et al., 2022). A previous study found that air pollution across Africa caused ~1.1 million deaths in 2019 (Fisher et al., 2021). However, the study of air quality in Africa is hindered by the scarcity of ground-based observations (e.g., Paton-Walsh et al., 2022), modelling capability and the use of satellite observations. In this paper, we will focus on air quality analyses over Africa with the new model Multi-Scale Infrastructure for Chemistry and Aerosols (MUSICA; Pfister et al., 2020).

Atmospheric chemistry modeling is a useful tool to perform research on air quality conditions and evolution. Various models have been applied to study atmospheric chemistry and air quality in Africa such as the Weather Research and Forecasting (WRF) model coupled with Chemistry (WRF-Chem) (e.g., Kuik et al., 2015; Kumar et al., 2022), the GEOS-Chem chemical transport model (e.g., Marais et al., 2012, 2019; Lacey et al., 2018), the CHIMERE chemical transport model (e.g., Menut et al., 2018; Mazzeo et al., 2022), and the U.K. Earth System Model (UKESM1) (Brown et al., 2022), and GEOS5 (Bauer et al., 2019).

MUSICA is a new state-of-the-art community modeling infrastructure that enables the study of atmospheric composition and chemistry across all relevant scales (Pfister et al., 2020). The newly developed MUSICA Version 0 (MUSICAv0) is a global chemistry-climate model that allows global simulations with regional refinement down to a few kilometers spatial resolution (Schwantes et al., 2022). The coupling with other components of the Earth system (e.g., land, ocean, and sea ice) can also be performed at multiple scales. MUSICAv0 has various advantages and is particularly suitable for research applications over Africa. For example, MUSICAv0 can be used to study the interactions between atmospheric chemistry and other components of the Earth system and climate. MUSICA also includes the whole atmosphere (from the surface to thermosphere), and therefore can also be used to study the stratosphere and above and interactions between the stratosphere and troposphere. This is critical because some of the environmental issues

https://doi.org/10.5194/gmd-2023-50
Preprint. Discussion started: 4 May 2023
© Author(s) 2023. CC BY 4.0 License.

Geoscientific Model Development Discussions

in Africa are coupled (e.g., the ozone–climate penalty; Brown et al., 2022). In addition, as a global model, MUSICAv0 does not require boundary conditions to study a region at high resolution. Global impacts and interactions can be simulated in a consistent and coherent way. This feature is important as inflow from other continents and oceans significantly impacts air quality in Africa. MUSICAv0 has been evaluated over North America (Schwantes et al., 2022, Tang et al., 2022) and is also being developed and tested in other regions around the globe (https://wiki.ucar.edu/display/MUSICA/Available+Grids).

This paper serves as the basis for the future application of MUSICAv0 in Africa. In this study, we develop a MUSICAv0 model grid with regional refinement over Africa. Because MUSICAv0 with Africa refinement is newly developed while WRF-Chem has been previously used for African atmospheric chemistry and air quality studies, here we include results from WRF-Chem to assess the ability of MUSICAv0 in reproducing the regional features of atmospheric composition as simulated by WRF-Chem. We conduct the MUSICAv0 simulation for the year 2017 to compare with a previous WRF-Chem simulation (Kumar et al., 2022). MUSICAv0 and the WRF-Chem simulation and the observational data used in this study are described in Section 2. The MUSICAv0 model simulation results are evaluated against in situ observations and compared with satellite retrievals in Section 3. In Section 4, we provide an example application of MUSICAv0 over Africa – identifying key potential regions in Africa for future in situ observations and field campaign(s).

2. Model and data

2.1 MUSICAv0

MUSICA is a newly developed framework for simulations of large-scale atmospheric phenomena in a global modeling framework, while still resolving chemistry at emission- and exposure-relevant scales (Pfister et al., 2020). MUSICA version 0 (MUSICAv0) is a configuration of the Community Earth System Model (CESM). It is also known as the Community Atmospheric Model with chemistry (CAM-chem) (Tilmes et al., 2019; Emmons et al., 2020) with regional refinement (RR) down to a few kilometers (Lauritzen et al., 2018; Schwantes et al., 2022). CAM-chem, and thus MUSICAv0, includes several choices of chemical mechanisms of varying complexity. This study uses the default MOZART-TS1 chemical mechanism for gas phase chemistry (including comprehensive tropospheric and stratospheric chemistry; Emmons et al., 2020) and the four-mode version of the Modal Aerosol Module (MAM4; Liu et al., 2016) for the aerosol scheme.

The MUSICAv0 users have the option to create their own model grid. MUSICAv0 is currently being developed and tested for applications over various regions globally (https://wiki.ucar.edu/display/MUSICA/Available+Grids), including North America, India, East Asia, South America, Australia, and Korea, among others. (e.g., Schwantes et al., 2022; Tang et al., 2022; Jo et al., 2023). In this study, we develop a model grid for applications in Africa (ne0np4.africa_v5.ne30x4). As shown in Figure 1a, the horizontal resolution is ~111 km × 111 km (i.e., 1° latitude × 1° equatorial longitude) globally, and ~28 km × 28 km (i.e., 0.25° latitude × 0.25° equatorial longitude) within the region over Africa. Our simulation uses the default option for vertical layers (i.e., 32 layers from the surface to ~3.64 hPa).

Here we run MUSICAv0 with the model grid for Africa for the year 2017, saving 3-hourly output. We use the Copernicus Atmosphere Monitoring Service Global Anthropogenic emissions, (CAMS-GLOB-ANTH) version 5.1 (Soulie et al., 2023) for anthropogenic emissions and the

https://doi.org/10.5194/gmd-2023-50
Preprint. Discussion started: 4 May 2023
© Author(s) 2023. CC BY 4.0 License.

Quick Fire Emissions Dataset (QFED) for fire emissions (Darmenov and da Silva, 2013). Plume rise climatology is applied to fire emissions following Tang et al. (2022). In addition, we also include open waste burning (https://www.acom.ucar.edu/Data/fire/; Wiedinmyer et al., 2014) emissions in the simulation. The model has the option of a free-running atmosphere or nudging to external meteorological reanalysis. In this simulation, only wind and temperature are nudged to the Modern-Era Retrospective analysis for Research and Applications, Version 2 (MERRA-2; Gelaro et al., 2017) with a relaxation time of 12 hours.

We also added carbon monoxide (CO) tracers in the simulation to understand the source and transport of air pollution. CO tracers in CAM-chem/MUSICAv0 are described in detail by Tang et al. (2019). In this study we include tracers for 6 regions (North Africa, West Africa, East Africa, Central Africa, Southern Africa, and the rest of the world) and 3 emission sources separately (anthropogenic emissions, fire emissions, and open waste burning emissions). In total, there are 18 tagged CO tracers.

2.2 WRF-Chem

The Weather Research and Forecasting (WRF) model coupled with Chemistry (WRF-Chem) is a regional chemical transport model. It has been widely used for air quality studies in Africa. In this study we use model results from a WRF-Chem simulation described by Kumar et al. (2022). The WRF-Chem simulation has a grid spacing of 20 km, slightly higher than the MUSICAv0 simulation, and the model domain is highlighted in Figure 1a. The simulation has 36 vertical levels from the surface to ~50 hPa. The WRF-Chem simulation uses the Model for Ozone and Related Tracers-4 (MOZART-4) chemical mechanism (Emmons et al., 2010) for tropospheric gas phase chemistry, and the Goddard Global Ozone Chemistry Aerosol Radiation and Transport (GOCART) model (Chin et al., 2002) for aerosol processes. The European Centre for Medium Range Weather Forecasts (ECMWF) global reanalysis (ERA-Interim) fields are used for initial and boundary meteorology conditions, while another CAM-chem simulation is used for initial and boundary chemical conditions (Kumar et al., 2022). The WRF-Chem simulation used the global Emission Database for Atmospheric Research developed for Hemispheric Transport of Air Pollution (EDGAR-HTAP v2) for anthropogenic emissions and the Fire Inventory from NCAR version 1.5 (FINNv1.5) (Wiedinmyer et al., 2011) for fire emissions. The WRF-Chem output is saved hourly, however we only use 3-hourly output to match the MUSICAv0 simulation.

2.3 ATom

The Atmospheric Tomography mission (ATom; Thompson et al. 2022) was designed to study the impact of human-produced air pollution on greenhouse gases, chemically reactive gases, and aerosols in remote ocean air masses. During the project, the DC-8 aircraft sampled the remote troposphere with continuous vertical profiles. There were four seasonal deployments from the summer of 2016 through the spring of 2018. Here we compare the MUSICAv0 simulation with observations from ATom-2 (January–February 2017) and ATom-3 (September–October 2017). Since the ATom flight tracks were mostly outside the WRF-Chem domain (Figure 1a), we do not compare the WRF-Chem simulation with ATom data. However, we compare chemical species from the MUSICAv0 simulation to the 2-minute merged ATom measurements globally to obtain a benchmark and broader understanding of MUSICAv0 performance both within and outside the refined region. The model output is saved along the ATom aircraft flight tracks and with respect to the observational times at run time. Nitric oxide (NO) and ozone (O_3) measurements from the NOAA Nitrogen Oxides and Ozone (NOyO3) instrument (Bourgeois et al., 2020, 2021) and the

https://doi.org/10.5194/gmd-2023-50
Preprint. Discussion started: 4 May 2023
© Author(s) 2023. CC BY 4.0 License.

merged CO data (from Quantum Cascade Laser System and NOAA Picarro CO measurements) are used.

2.4 IAGOS

The In-service Aircraft for a Global Observing System (IAGOS) is a European research infrastructure, and was developed for operations on commercial aircraft to monitor atmospheric composition (Petzold et al., 2015). The IAGOS instrument package 1 measures CO, O_3, air temperature, and water vapor (https://www.iagos.org/iagos-core-instruments/package1/). CO is measured by infrared absorption using the gas filter correlation technique (Precision: ±5%, Accuracy: ±5 ppb) while O_3 is measured by UV absorption at 253.7 nm (Precision: ±2%, Accuracy: ±2 ppb). We use airborne measurements of CO, O_3, air temperature, and water vapor from IAGOS for model evaluation. The locations of the IAGOS flight tracks over Africa are shown in Figure 1b. The model results and IAGOS data comparisons are conducted separately for five African sub-regions (defined in Figure 1b).

2.5 Ozonesondes

The ozonesonde is a balloon-borne instrument that measures atmospheric O_3 profiles through the electrochemical concentration cell using iodine/iodide electrode reactions (Thompson et al., 2017), with records of temperature, pressure, and relative humidity from standard radiosondes. We use ozonesonde data from Southern Hemisphere ADditional OZonesondes (NASA/GSFC SHADOZ; Thompson et al., 2017; Witte et al., 2017, 2018). Specifically, ozonesonde data from four sites are used (Figure 1b): Ascension (Ascension Island, U.K.), Nairobi (Kenya), Irene (South Africa), and La Reunion (La Réunion Island, France). The average O_3 measurement uncertainty ranged from 5–9% for the ozonsonde data used in this study.

2.6 WDCGG

Monthly surface CO measurements from the World Data Center for Greenhouse Gases (WDCGG; operated by the Japan Meteorological Agency in collaboration with the World Meteorological Organization) are used for model evaluation. Data from six sites are used (Figure 1b), namely (Ascension Island, U.K.), Assekrem (Algeria; remote site located in Saharan desert), Gobabeb (Namibia; located at the base of a linear sand dune, next to an interdune plain), Cape Point (South Africa; site exposed to the sea on top of a cliff 230 meters above sea level), Izana (Tenerife, Spain; located on the Island that is ~300 km west of the African coast), and Mare (Seychelles; near an international airport).

2.7 Surface $PM_{2.5}$

At the U.S. embassies, regulatory-grade monitoring data are collected with Beta Attenuation Monitors (BAMs), using a federal equivalent monitoring method, with an accuracy within 10% of federal reference methods (Watson et al., 1998; U.S. EPA, 2016). These instruments are operated by the U.S. State Department and the U.S. EPA, and data are available through AirNow (https://www.airnow.gov/international/us-embassies-and-consulates/). We use the measurements at the U.S. embassy locations in Addis Ababa Central (Ethiopia, 9.06° N, 38.76° E) and Kampala (Uganda, 0.30° N, 32.59° E) for the year 2017 as references (Malings et al., 2020) to match our simulations. The raw data are made available hourly and for this study we use daily mean $PM_{2.5}$ for comparison with model simulations.

https://doi.org/10.5194/gmd-2023-50
Preprint. Discussion started: 4 May 2023
© Author(s) 2023. CC BY 4.0 License.

Geoscientific Model Development Discussions

2.8 MOPITT

The Measurements of Pollution in the Troposphere (MOPITT) instrument on board the NASA Terra satellite provides both thermal-infrared (TIR) and near-infrared (NIR) radiance measurements since March 2000. Retrievals of CO column density and vertical profiles are provided in a multispectral TIR–NIR joint product which has sensitivity to near-surface as well as free tropospheric CO (Deeter et al., 2011; Worden et al., 2010). Here we use the MOPITT Version 9 Level 2 CO column product (Deeter et al., 2022) over Africa to evaluate the MUSICAv0 and WRF-Chem simulations. MOPITT Version 9 has significant updates to the cloud detection algorithm and NIR calibration scheme. The MOPITT satellite pixel size is ~22 km × 22 km, and the overpass time is ~10:30 am local time in 2017. When comparing model outputs to MOPITT the recommended data quality filter is applied and model outputs are interpolated to the MOPITT retrievals in space and time. To perform quantitative comparisons, the MOPITT averaging kernel and a priori are used to transform the model CO profiles to derive model column amounts.

2.9 OMI NO_2 (QA4ECV)

Tropospheric column NO_2 from the Ozone Monitoring Instrument (OMI) on board Aura is compared to the model in this study. Specifically, the NO_2 product from the quality assurance for the essential climate variables (QA4ECV) project is used (Boersma et al., 2017a; Compernolle et al., 2020). The satellite pixel size is ~13 km × 25 km, and the overpass time is ~1:40 pm local time in 2017. A data quality filter was applied following the Product Specification Document (Boersma et al., 2017b; processing_error_flag = 0, solar_zenith_angle < 80, snow_ice_flag < 10 or snow_ice_flag = 255, amf_trop/amf_geo > 0.2, and cloud_radiance_fraction_no20 <= 0.5). Model profiles were transformed using the provided tropospheric air mass factor (AMF) and averaging kernels.

2.10 OMI HCHO (QA4ECV)

We also use tropospheric column HCHO from OMI in this study. Similar to OMI NO_2, we also use OMI HCHO product from QA4ECV (De Smedt et al., 2017a). A data quality filter was applied following the Product User Guide (De Smedt et al., 2017b; processing_error_flag = 0 and processing_quality_flag = 0). Model profiles were transformed using provided averaging kernels. We note that HCHO retrievals are subject to relatively large uncertainties compared to other satellite products used in this study. Therefore, the comparisons between model results and the OMI HCHO product only indicate the model-satellite discrepancies rather than determining model deficiencies. In addition, the WRF-Chem simulation from Kumar et al. (2022) does not include HCHO in the output and hence will not be compared.

2.11 MODIS AOD

The aerosol optical depth (AOD) product (550 nm) from the Moderate Resolution Imaging Spectroradiometer (MODIS) on board Terra NASA Terra satellite is used. Specifically, we used the MODIS Level 2 Collection 6.1 product (MOD04_L2; Levy et al., 2017). Deep Blue Aerosol retrievals are used (Hsu et al., 2013; Levy et al., 2013) to include retrievals over the desert. The MODIS satellite pixel size is ~1 km × 1 km, and the overpass time is ~10:30 am local time.

3. Model comparisons with satellite data and evaluation with in situ observations

Africa includes a wide range of environments and emissions source. Therefore, in this section we separate the continent in five sub-regions for analysis following Kumar et al. (2022).

https://doi.org/10.5194/gmd-2023-50
Preprint. Discussion started: 4 May 2023
© Author(s) 2023. CC BY 4.0 License.

CO is a good tracer of anthropogenic and biomass burning emissions and modeled CO tracers are used in this section to understand sources. Figure 2 shows the seasonal averages of CO column distributions over Africa from MOPITT along with the MUSICAv0 and WRF-Chem biases. The highest levels of CO in these maps are primarily associated with biomass burning, which moves around the continent with season. Both MUSICAv0 and WRF-Chem simulations underestimate the CO column compared to MOPITT (Figures 3a and 3b). Overall, MUSICAv0 agrees better with the OMI tropospheric NO_2 column (Figure 3c) and MODIS AOD (Figure 3e) than WRF-Chem (Figures 3d and 3f). The MUSICAv0 simulation overall has lower tropospheric HCHO column than OMI in all regions and seasons (Figure 3g). Spatial distributions of model biases against the OMI tropospheric NO_2 column, MODIS AOD, and OMI tropospheric HCHO column are included in Figures S1–S3. In this section we compare the model results with satellite data and in situ observations over sub-regions in Africa and oceans near Africa (Figure 1b).

3.1 North Africa

Over North Africa, both MUSICAv0 and WRF-Chem simulations underestimate the CO column during 2017 (Figures 2 and 3). As shown by the tagged model CO tracers (Figure 4), CO over North Africa is mainly driven by transport of CO from outside the continent and anthropogenic emissions. The model underestimation compared to the MOPITT CO column is consistent with the results of the comparisons with surface CO observations from WDCGG at the two sites located in North Africa (Assekrem and Izana; Figures 5a and 5c). At the two surface sites, the composition of source types and source regions are close to the composition of source types and source regions of the column average over North Africa (Figure 4 and Figures S4 and S5), hence the two sites are representative of the background conditions of North Africa. Compared to MODIS AOD, WRF-Chem has a mean bias of 0.36 whereas MUSICAv0's mean bias is 0.17 for 2017. The model AOD biases over North Africa are likely driven by dust. No comparison is made with IAGOS O_3 in North Africa due to data availability.

3.2 West Africa

Over West Africa, fire and anthropogenic emissions are both important for CO pollutant and fire impacts peak in DJF (December, January, and February). Compared to the MOPITT CO column, the mean bias of MUSICAv0 and WRF-Chem for West Africa peak around February – the dry season of the Northern Hemisphere (Figure 3). In February, the MUSICAv0 mean bias is -1.1×10^{18} molecules/cm^2 and WRF-Chem mean bias is -7.5×10^{17} molecules/cm^2, which are likely driven by fire emission sources (Figure 4). Model comparisons with IAGOS CO also show a similar bias – both model simulations underestimate CO at all vertical levels. The underestimation peaks during DJF and below 600 hPa (Figure 6). As for MODIS AOD, WRF-Chem has the mean bias 0.69 whereas MUSICAv0's mean bias is 0.15, respectively. Similar to North Africa, the model biases in AOD over West Africa are also likely driven by dust and biomass burning. We also compare modeled O_3 with IAGOS O_3 observations (Figure 7).

Over West Africa, both models agree well with the IAGOS O_3 observations below 800 hPa (mean bias ranges from -1 to -4 ppb). Above 800 hPa over West Africa, WRF-Chem underestimates O_3 while MUSICAv0 overestimates O_3. Overall, MUSICAv0 consistently overestimates O_3 above 800 hPa in all seasons while the direction of WRF-Chem bias changes with seasons (Figure 7). When MUSICAv0 overestimates O_3, the bias is in general larger at the higher altitude of the troposphere. The concentration of the model stratospheric ozone tracer, O3S, is also larger at the higher altitude in DJF (Figure 9). The correlation of modeled O_3 and O3S is

https://doi.org/10.5194/gmd-2023-50
Preprint. Discussion started: 4 May 2023
© Author(s) 2023. CC BY 4.0 License.

Geoscientific Model Development Discussions

0.54, and the correlations of O_3S and model O_3 bias (modeled O_3 minus IAGOS O_3) is 0.35 over West Africa, implying the overestimation of O_3 in the upper troposphere could be partially driven by too strong stratosphere-to-troposphere flux of ozone. Lightning NO emissions can also impact O_3 in the upper troposphere. The MUSICAv0 simulation has somewhat (~3 times) higher lightning NO emissions (Figure S6) compared to a standard CAM-chem simulation (not shown), therefore the high ozone in the upper troposphere may be due to an over-estimate of lightning NO. Impacts of lightning NO emissions on upper troposphere O_3 in MUSICAv0 will be investigated and evaluated further in the future. A brief comparison with IAGOS measurements of air temperature and water vapor profiles over West Africa as well as other sub-regions shows that MUSICAv0 overall agrees well with these meteorological variables (Figure S7).

3.3 Central Africa

Compared to MOPITT CO column, the mean bias of MUSICAv0 and WRF-Chem for Central Africa varies with seasons (Figure 3) but peaks during the dry season in September (MUSICAv0 mean bias of -1.0×10^{18} molecules/cm^2; WRF-Chem mean bias of -1.2×10^{18} molecules/cm^2). The tagged model CO tracers show that in September, local fire emissions are the dominant driver of CO in Central Africa (Figure 4). Compared to the IAGOS CO profiles (Figure 6), both models have the largest bias over Central Africa among the sub-regions in Africa – mean bias of MUSICAv0 and WRF-Chem are -46 ppb and -36 ppb, respectively. The high bias over Central Africa mainly occurs during the fire season. In central Africa, both models also underestimate NO_2 (mean biases of MUSICAv0 and WRF-Chem are -1.5×10^{14} and -5.5×10^{14} molecules/cm^2, respectively). The underestimations in both CO and NO_2 by the two model simulations are likely driven by the underestimation in fire emissions. Indeed, the emission estimates from the newest version of FINN (FINNv2.5; Wiedinmyer et al., 2023) are higher compared to both QFED (used in the MUSICAv0 simulation) and FINNv1.5 (used in the WRF-Chem simulation) in this region.

Model mean bias of HCHO (-1.3×10^{16} molecules/cm^2 for the whole 2017) over Central Africa is the largest among the five regions (Figure 3). The spatial distribution of HCHO bias (Figure S4) largely co-locates with the vegetation (Figure 8). Over the barren or sparsely vegetated area in North Africa and along the west coast of Southern Africa, HCHO biases are relatively small while over the vegetated area HCHO bias are relatively large. Over North Africa, the mean bias is -0.66×10^{16} molecules/cm^2 for the whole 2017 whereas over the other four regions, the mean bias ranges from -0.93×10^{16} molecules/cm^2 to -1.31×10^{16} molecules/cm^2 for the whole 2017. This indicates that the negative bias in MUSICAv0 HCHO could be due to underestimated biogenic emissions in the model. In addition, the underestimation of HCHO in Central Africa (Figure S4) co-locates with the underestimation of CO during fire season (Figure S1), implying that fire emissions may also contribute to the HCHO underestimation in MUSICAv0. It is important to note that the uncertainty of OMI tropospheric HCHO column is relatively large compared to other satellite products. Here the averaged retrieval uncertainty (random and systematic) is ~120%.

When compared to the IAGOS O_3 profiles over Central Africa (Figure 7), both models agree well with the IAGOS O_3 observations below 800 hPa (mean bias ranges from -1 to -4 ppb). Above 800 hPa, WRF-Chem underestimates O_3 while MUSICAv0 overestimates O_3. The correlation of modeled O_3 and O3S is 0.67, and the correlations of O_3S and model O_3 bias is 0.50 over Central Africa, indicating O_3 overestimation in Central Africa are more likely to be impacted by stratosphere-to-troposphere flux of ozone than that in West Africa.

https://doi.org/10.5194/gmd-2023-50
Preprint. Discussion started: 4 May 2023
© Author(s) 2023. CC BY 4.0 License.

3.4 East Africa

CO over East Africa is dominated by local emissions and inflow from outside the continent. Fire and anthropogenic emissions contribute approximately the same to CO over East Africa (Figure 4). Both MUSICAv0 and WRF-Chem simulations underestimate the CO column compared to MOPITT (Figure 3), and the WRF-Chem simulation also underestimate the tropospheric NO_2 column compared to OMI. The biases in CO column and tropospheric NO_2 column peak in September, likely driven by fire emissions (Figure 4).

Compared to IAGOS O_3 profiles over East Africa, biases of MUSICAv0 below 600 hPa has a seasonal variation while over 600 hPa are consistently positive (Figure 7). The correlations of O_3S and model O_3 bias against IAGOS data is 0.50 in the region. The correlations between O_3S and model O_3 bias are highest over Central and East Africa compared to other regions, indicating stratosphere influence are strongest in these two regions among the sub-regions. Central and East Africa are relatively more mountainous therefore topography driven stratospheric intrusions might be expected. The Nairobi ozonesonde site is located in East Africa (Figure 1b). When comparing to the O_3 profiles from ozonesondes (Figure 9), MUSICAv0 overall overestimates O_3 in the troposphere at the four sites while WRF-Chem tends to underestimate O_3 in the free troposphere (below 200 hPa). The Nairobi site is an exception where both MUSICAv0 and WRF-Chem simulations significantly overestimate O_3 in all seasons (mean bias of MUSICAv0 and WRF-Chem below 200 hPa are 27 ppb and 20 ppb, respectively). Among the four ozonesonde sites, correlations of model bias of O_3 and O_3S are highest at the Nairobi site (0.74) where the model significantly overestimates O_3. The results of model-ozonesonde comparisons are consistent with the results of model-IAGOS comparisons and indicate a potential issue in modeled stratosphere-to-troposphere flux of ozone.

There are two surface $PM_{2.5}$ sites in East Africa (Addis Ababa and Kampala; Figure 1b). Despite using different aerosol methods and emission inventories, both MUSICAv0 and WRF-Chem underestimate surface $PM_{2.5}$ when compared to observations at the two sites (Figure 10). The errors in $PM_{2.5}$ concentrations at the U.S. Embassy in Kampala are especially prominent. However, both models approximate the variation of the $PM_{2.5}$ in both locations. Many factors contribute to the inconsistency in the magnitude of modeled $PM_{2.5}$ concentrations. For instance, emission inventories in this region require additional improvement. In Uganda, increasing motor vehicle ownership and burning biomass for domestic energy use contribute to ambient $PM_{2.5}$ levels (Clarke et al., 2022; Petkova et al., 2013). Detailed $PM_{2.5}$ composition measurements would also help to pinpoint the cause of inaccuracies. In addition, model resolutions could also be a potential reason for the underestimation.

3.5 Southern Africa

Among the five regions, MUSICAv0 has the lowest mean bias (-3.2×10^{17} molecules/cm^2 annually) over Southern Africa (Figure 3). WRF-Chem also has low mean bias and RMSE over Southern Africa except for the months of September, October, and November (SON) period where WRF-Chem has larger CO mean bias (-6.2×10^{17} molecules/cm^2) than MUSICAv0. Tagged model CO tracers indicate that CO over Southern Africa is significantly impacted by CO emissions from Central Africa, East Africa, Southern Africa, and inflow from outside the continent. As for the source types, anthropogenic and fire emissions are both important and fire impacts peak in September. There are two WDCGG sites located in Southern Africa (Figure 1b; Gobabeb and Cape Point). When compared to surface CO observations from WDCGG, both models consistently underestimate CO by up to 40% at most sites. The Cape Point site in Southern Africa is an

https://doi.org/10.5194/gmd-2023-50
Preprint. Discussion started: 4 May 2023
© Author(s) 2023. CC BY 4.0 License.

exception (Figure 5) where MUSICAv0 overestimates CO by 40 ppb (annual mean; and up to 78 ppb in May 2017). CO tracers in the model (Figures S4 and S5) show that CO at Cape Point is mainly driven by anthropogenic CO emissions from Southern Africa. Therefore, the overestimation of CO by MUSICAv0 should be due to the overestimation of anthropogenic emissions from Southern Africa used in the model. As for NO_2, WRF-Chem underestimates tropospheric NO_2 column in most regions except for Southern Africa (Figure 3). Over Southern Africa, WRF-Chem overestimates NO_2 especially during June, July, and August (JJA). MUSICAv0 also tends to overestimates NO_2 at the same location in JJA however the bias is not as large as for WRF-Chem.

MUSICAv0 simulation overall has a lower mean bias (0.14 annually) than the WRF-Chem simulation (mean bias of 0.31 annually) compared to MODIS AOD with Southern Africa being the only exception (Figure 3). Over Southern Africa, MUSICAv0 overestimates AOD by ~0.21 annually (Figure 3) and the bias peaks in January (mean bias=0.45). This overestimation in AOD over Southern Africa is not seen in WRF-Chem. It is likely that the MUSICAv0 overestimation in AOD over Southern Africa is also due to biases in modeled dust as the AOD bias is co-located with the only barren or sparsely vegetated area in Southern Africa (Figure 8 and Figure S3).

Over Southern Africa, MUSICAv0 tends to overestimate O_3 compared to IAGOS at all levels at all seasons in 2017 (Figure 7). The concentration of O3S over Southern Africa is higher than those over other regions. However, the correlation of O_3S and model O_3 bias is lower than other regions (0.13) indicating stratosphere-to-troposphere flux of ozone may not be the main driver of O_3 bias over Southern Africa even though stratosphere-to-troposphere flux of ozone are relatively strong in the region. The Irene ozonesonde site is located in Southern Africa (Figure 1b). Compared to the ozonesonde O_3 profiles at the Irene site, however, the MUSICAv0 performance has a seasonal variation (Figure 9e-9h). Compared to other ozonesonde sites, the correlation of O_3S and model O_3 bias over Southern Africa is lower (0.14) and MUSICAv0 agrees relatively well with observations, which is consistent with the comparison results with IAGOS data (Figure 7).

3.6 Oceans near Africa

We compare the CO, NO, and O_3 from the MUSICAv0 simulation with measurements from ATom-2 and ATom-3 in 2017 (Figure 1a) to provide a global benchmark. Measurements made over the Atlantic Ocean and Pacific Ocean, and in January-February (Jan-Feb) and September-October (Sep-Oct) are compared separately (Figures 11 and 12). The comparison was made with data averaged into 10° latitude and 200 hPa bins. Overall, the model consistently underestimates CO globally in both seasons. The underestimation of CO is a common issue in atmospheric chemistry models and could be due to various reasons, including emissions, deposition, and chemistry (e.g., Fisher et al., 2017; Shindell et al., 2006; Stein et al., 2014; Tilmes et al., 2015; Tang et al., 2018; Gaubert et al., 2020). Specifically for our MUSICAv0 simulation in this study, the model bias in CO is relatively large (up to 52 ppb) over the Northern Hemisphere (especially at high latitude and near the surface) and small over the Southern Hemisphere (Figures 11 and 12). Over the Atlantic Ocean, the bias in CO is larger in September-October than Jan-Feb in both the Northern Hemisphere (-30 ppb in Jan-Feb versus -34 ppb in Sep-Oct) and Southern Hemisphere (-11 ppb in Jan-Feb versus -14 ppb in Sep-Oct). Over the Pacific Ocean, however, the CO bias is similar for both time periods in the Northern Hemisphere (-30 ppb) while in the Southern Hemisphere, the CO bias changes significantly from -8 ppb in Jan-Feb to -16 ppb in Sep-Oct. The changes in CO bias over the Southern Hemisphere are likely due to seasonal change in fire emissions. Overall, the mean biases (Figures 11 and 12) suggest that the simulation agrees

https://doi.org/10.5194/gmd-2023-50
Preprint. Discussion started: 4 May 2023
© Author(s) 2023. CC BY 4.0 License.

Geoscientific Model Development Discussions

better with ATom observations in the Southern Hemisphere than in the Northern Hemisphere, and in Jan-Feb than in Sep-Oct (Figures 11 and 12), consistent with Gaubert et al. (2016).

In both seasons and both hemispheres, the model in general overestimates O_3 in the stratosphere/UTLS (upper troposphere and lower stratosphere) by up to 38 ppb (above 200 hPa). In the troposphere (below 200 hPa), the model overall agrees well with the ATom data over the Pacific Ocean in the Southern Hemisphere (in most cases the bias is less than ±5 ppb). However, over the Atlantic Ocean in the Southern Hemisphere, MUSICAv0 tends to overestimate O_3, especially in Jan-Feb. In the troposphere of the Northern Hemisphere, MUSICAv0 consistently overestimates O_3 over both oceans and both seasons. The positive bias in O_3 decreases from the upper troposphere towards the surface, indicating that the overestimation of O_3 in the troposphere may be due to stratosphere-to-troposphere flux of ozone. This was also noted for other global models (Bourgeois et al. 2021). As for NO, the model tends to overestimate NO above 200 hPa (approximately the stratosphere and Upper Troposphere-Lower Stratosphere; UTLS) by up to 50 ppt. Overall, the NO biases can be either positive or negative depending on location and season. The distributions of NO bias (Figures 11 and 12) do not show an overall spatial pattern, unlike those for CO (which changes monotonically with latitude) or O_3 (which changes monotonically with altitude).

4. Model application: identifying key regions in Africa for future in situ observations and field campaign(s)

As a demonstration of the application of MUSICAv0, here we use the results of model-satellite comparisons to identify potential regions where the atmospheric chemistry models need to be improved substantially. More field campaigns and more in situ observations would not only provide observational benchmark dataset to understand and improve the modeling capability in the region, but would be also useful for the validation and calibration of satellite products. Here we use Taylor score to quantify model-satellite discrepancies. Taylor score (Taylor, 2001) is defined by

$$S = \frac{4(1+R)}{(\hat{\sigma}_f+1/\hat{\sigma}_f)^2(1+R_0)}$$

where $\hat{\sigma}_f$ is the ratio of σ_f (standard deviation of the model) and σ_r (standard deviation of observations), R is correlation between model and observations, and R_0 is the maximum potentially realizable correlation (=1 in this study). Taylor score ranges from 0 to 1 and a higher Taylor score indicates better satellite-model agreement. To identify potential locations, we separate the Africa continent into 5° × 5° (latitude × longitude) pixels as shown in Figure 13. And for each pixel, we calculate Taylor scores of MUSICAv0 compared to the three satellite Level 2 products (e.g., MOPITT CO column retrievals, OMI tropospheric NO_2 column retrievals, and MODIS AOD) separately. And then three Taylor scores are summed up to obtain the total Taylor score for MUSICAv0 (ranges from 0 to 3) as shown in Figures 13a-13e. A similar calculation is conducted for WRF-Chem (Figures 13f-13j). Note that we did not include Taylor scores for HCHO in the total Taylor score due to that (1) WRF-Chem simulations did not save HCHO output, and (2) the HCHO retrievals have relatively high uncertainties (Taylor scores of MUSICAv0 compared to OMI tropospheric HCHO column retrievals are provided separately in Figure S8).

Overall, both MUSICAv0 and WRF-Chem have low total Taylor scores in the 30°E – 45°E, 5°S – 5°N region in East Africa (a region of 15° longitude × 10° latitude) during MAM (March, April, and May), JJA (June, July, and August), and SON (September, October, and November), as

https://doi.org/10.5194/gmd-2023-50
Preprint. Discussion started: 4 May 2023
© Author(s) 2023. CC BY 4.0 License.

highlighted in Figure 13, indicating relatively large model-satellite discrepancies in the region. Moreover, this is also the region where the Nairobi ozonesonde site and the Kampala surface $PM_{2.5}$ site are located (Figure 1b). As discussed above, both MUSICAv0 and WRF-Chem significantly overestimate O_3 (Figure 9) and largely underestimate $PM_{2.5}$ (Figure 10) in the region. More in situ observations or future field campaigns in the region can substantially help in the understanding model-satellite and model-in situ observation discrepancies and improving model performance.

The 30°E – 45°E, 5°S – 5°N region in East Africa is potentially a favorable location for future field campaign(s) not only because of the large model-satellite and model-in situ observation discrepancies, but also due to that the population density is high and landcover are diverse in the region (Figure 8). The relatively high population density in the region indicates that improved air quality modeling in the region can benefit a large population. And a diverse landcover indicates more processes/environments can be sampled. CO tracers in the model (Figure 14) show that CO over the region is mainly driven by both anthropogenic and fire emissions. Anthropogenic emissions play a more important role in this region compared to East Africa in general (Figures 4 and 14). In terms of source regions, emissions from East Africa and inflow from outside the continent are the dominant source, with some contributions from Central Africa. Note that the source analyses using model tracers may be subject to uncertainties in the emission inventories. As discussed above (e.g., Section 3.4), there might be missing sources in the region. Therefore, a field campaign in the region can help address this issue.

We would like to point out that in this analysis, the key area is selected using 3 satellite products/chemical species and two models. The Taylor score is a comprehensive measure of model performance that accounts for variance and correlation, however, other models and types of comparisons may provide different answers.

5. Conclusions

Africa is one of the most rapidly changing regions in the world and air pollution is a growing issue at multiple scales over the continent. MUSICAv0 is a new community modeling infrastructure that enables the study of atmospheric composition and chemistry across all relevant scales. We developed a MUSICAv0 grid with Africa refinement (~28 km × 28 km over Africa and ~110 km × 110 km for the rest of the world) and conducted the simulation for the year 2017. We evaluated the model with in situ observations including ATom-2 and ATom-3 airborne measurements of CO, NO, and O_3, IAGOS airborne measurements of CO and O_3, O_3 profiles from ozonesondes, surface CO observations from WDGCC, and surface $PM_{2.5}$ observations from two U.S. Embassy locations. We then compare MUSICAv0 with satellite products over Africa, namely MOPITT CO column, MODIS AOD, OMI tropospheric NO_2 column, and OMI tropospheric HCHO column. Results from a WRF-Chem simulation were also included in the evaluations and comparisons as a reference. Lastly, as an application of the model, we identified potential African regions for in situ observations and field campaign(s) based on model-satellite discrepancies (quantified by Taylor score), with regard to model-in situ observation discrepancies, source analyses, population, and land cover. The main conclusions are as follows.

(1) When comparing to ATom-2 and ATom-3, MUSICAv0 consistently underestimates CO globally. Overall, the negative model bias increases with latitude from the Southern Hemisphere to the Northern Hemisphere. MUSICAv0 also tends to overestimate O_3 in the stratosphere/UTLS, and the positive model bias overall decreases with altitude.

https://doi.org/10.5194/gmd-2023-50
Preprint. Discussion started: 4 May 2023
© Author(s) 2023. CC BY 4.0 License.

(2) The MUSICAv0 biases in O_3 when compared to ATom, IAGOS, and ozonesondes are likely driven by stratosphere-to-troposphere fluxes of O_3 and lightning NO emissions.

(3) Overall, the performance of MUSICAv0 and WRF-Chem are similar when compared to the surface CO observations from six WDCGG sites in Africa.

(4) Both models have negative bias compared to the MOPITT CO column, especially over Central Africa in September, which is likely driven by fires.

(5) Overall, MUSICAv0 agrees better with OMI tropospheric NO_2 column than WRF-Chem.

(6) MUSICAv0 overall has a lower tropospheric HCHO column than OMI retrievals in all regions and seasons. Biogenic and fire emissions are likely to be the main driver of this disagreement.

(7) Over Africa, the MUSICAv0 simulation has smaller mean bias and RMSE compared to MODIS AOD than the WRF-Chem simulation.

(8) The 30°E – 45°E, 5°S – 5°N region in East Africa is potentially a favorable location for future field campaign(s) not only because of the large model-satellite and model-in situ observation discrepancies, but also due to the population density, landcover, and pollution source in this region.

Overall, the performance of MUSICAv0 is comparable to WRF-Chem. The underestimation of CO is a common issue in atmospheric chemistry models such as MUSICAv0 and WRF-Chem. The overestimation of O_3 in MUSICAv0 is likely driven by too strong of stratosphere-to-troposphere fluxes of O_3 and perhaps an over-estimate of lightning NO emissions, however, future studies are needed to confirm and solve this issue. The significant underestimation in surface $PM_{2.5}$ at two sites in East Africa and the overall overestimation in AOD in Africa compared to MODIS imply missing local sources and an overestimation of dust emissions, and require further study. Field campaigns and more in situ observations in 30°E–45°E, 5°S–5°N region in East Africa are necessary for the improvement of atmospheric chemistry model(s) as shown by the MUSICAv0 and WRF-Chem simulations. In the future, we plan to conduct a model simulation for multiple years and develop additional model grids with potentially higher resolution in Africa sub-regions based on the current MUSICAv0 Africa grid.

Code and data availability

The MUSICAv0 model source code and the model documentation can be downloaded through https://wiki.ucar.edu/display/MUSICA/MUSICA+Home (last access: 3 April 2023). CAMS-GLOB-ANTH version 5.1 emissions can be found at https://eccad3.sedoo.fr/data (last access: 3 April 2023). QFED emissions can be found at https://portal.nccs.nasa.gov/datashare/iesa/aerosol/emissions/QFED/ (last access: 3 April 2023). MERRA-2 data can be found at https://disc.gsfc.nasa.gov/datasets?project=MERRA-2 (last access: 3 April 2023). ATom data are available at https://espoarchive.nasa.gov/archive/browse/atom (last access: 3 April 2023). WDCGG data are available at https://gaw.kishou.go.jp/ (last access: 3 April 2023). IAGOS data are available at https://www.iagos.org/iagos-data/ (last access: 3 April 2023). NASA/GSFC SHADOZ data are available at https://tropo.gsfc.nasa.gov/shadoz/ (last access: 3 April 2023). The surface $PM_{2.5}$ data

https://doi.org/10.5194/gmd-2023-50
Preprint. Discussion started: 4 May 2023
© Author(s) 2023. CC BY 4.0 License.

used in this study are available through data are available through https://www.airnow.gov/international/us-embassies-and-consulates/ (last access: 3 April 2023). MOPITT CO and MODIS AOD data can be accessed through https://search.earthdata.nasa.gov/search (last access: 3 April 2023). OMI NO_2 and OMI HCHO data are available at https://www.temis.nl/qa4ecv/no2.html (last access: 3 April 2023) and https://www.temis.nl/qa4ecv/hcho.html (last access: 3 April 2023), respectively.

Acknowledgement

This material is based upon work partially supported by the National Aeronautics and Space Administration under Grant No. 80NSSC23K0181 issued through the NASA Applied Sciences SERVIR program. We thank ATom, WDCGG, IAGOS, NASA/GSFC SHADOZ teams, and the U.S. State Department and the U.S. EPA for in situ observations. We thank Anne Thompson and Gonzague Romanens for detailed explanation of SHADOZ Ozonesonde data format. We thank MOPITT, MODIS AOD, OMI NO_2 and OMI HCHO teams for the satellite products. The NCAR MOPITT project is supported by the National Aeronautics and Space Administration (NASA) Earth Observing System (EOS) program. We thank the QA4ECV project. We thank Sabine Darras for CAMSv5.1 emissions. We would like to acknowledge high-performance computing support from Cheyenne (doi:10.5065/D6RX99HX) provided by NCAR's Computational and Information Systems Laboratory, sponsored by the National Science Foundation. This material is based upon work supported by the National Center for Atmospheric Research, which is a major facility sponsored by the National Science Foundation under Cooperative Agreement No. 1852977. We thank James Hannigan, Ivan Ortega, Siyuan Wang, and all the attendees of ACOM CAM-chem/MUSICA weekly meeting for helpful discussions.

Competing interests

The contact author has declared that neither they nor their co-authors have any competing interests.

Author contributions

WT, LKE, HMW, and PL were involved in the initial design of this study. WT led the analysis. RK and CH conducted the WRF-Chem simulation. ZZ interpretated $PM_{2.5}$ results. BG, ST, SM and other coauthors provide discussions. RRB helped with QFED emissions. CG and AS produced CAMSv5.1 emissions. KM, BCD, JP, and CT conducted measurements during ATom. WT prepared the paper with improvements from all coauthors.

Reference

Baudoin, M.A., Vogel, C., Nortje, K. and Naik, M., 2017. Living with drought in South Africa: lessons learnt from the recent El Niño drought period. International journal of disaster risk reduction, 23, pp.128-137.

Bauer, S. E., Im, U., Mezuman, K., & Gao, C. Y. (2019). Desert dust, industrialization, and agricultural fires: Health impacts of outdoor air pollution in Africa. *Journal of Geophysical Research: Atmospheres*, 124, 4104– 4120. https://doi.org/10.1029/2018JD029336.

https://doi.org/10.5194/gmd-2023-50
Preprint. Discussion started: 4 May 2023
© Author(s) 2023. CC BY 4.0 License.

631 Boone, A.A., Xue, Y., De Sales, F., Comer, R.E., Hagos, S., Mahanama, S., Schiro, K., Song, G.,
632 Wang, G., Li, S. and Mechoso, C.R., 2016. The regional impact of Land-Use Land-cover Change
633 (LULCC) over West Africa from an ensemble of global climate models under the auspices of the
634 WAMME2 project. Climate Dynamics, 47(11), pp.3547-3573.

635 Brown, F., Folberth, G. A., Sitch, S., Bauer, S., Bauters, M., Boeckx, P., Cheesman, A. W., Deushi,
636 M., Dos Santos Vieira, I., Galy-Lacaux, C., Haywood, J., Keeble, J., Mercado, L. M., O'Connor,
637 F. M., Oshima, N., Tsigaridis, K., and Verbeeck, H., 2022. The ozone–climate penalty over South
638 America and Africa by 2100, Atmos. Chem. Phys., 22, 12331–12352, https://doi.org/10.5194/acp-
639 22-12331-2022.
640
641 Boersma, K. F., Eskes, H., Richter, A., De Smedt, I., Lorente, A., Beirle, S., Van Geffen, J., Peters,
642 E., Van Roozendael, M. and Wagner, T., (2017a). QA4ECV NO2 tropospheric and stratospheric
643 vertical column data from OMI (Version 1.1). Royal Netherlands Meteorological Institute
644 (KNMI). http://doi.org/10.21944/qa4ecv-no2-omi-v1.1.
645
646 Boersma, K.F., van Geffen, J., Eskes, H., van der A, R., De Smedt, I. and Van Roozendael, M.,
647 2017b. Product specification document for the QA4ECV NO2 ECV precursor product.
648
649 Bourgeois, I., Peischl, J., Thompson, C. R., Aikin, K. C., Campos, T., Clark, H., Commane, R.,
650 Daube, B., Diskin, G. W., Elkins, J. W., Gao, R.-S., Gaudel, A., Hintsa, E. J., Johnson, B. J., Kivi,
651 R., McKain, K., Moore, F. L., Parrish, D. D., Querel, R., Ray, E., Sánchez, R., Sweeney, C.,
652 Tarasick, D. W., Thompson, A. M., Thouret, V., Witte, J. C., Wofsy, S. C., and Ryerson, T. B.:
653 Global-scale distribution of ozone in the remote troposphere from the ATom and HIPPO airborne
654 field missions, Atmos. Chem. Phys., 20, 10611–10635, https://doi.org/10.5194/acp-20-10611-
655 2020, 2020.
656
657 Bourgeois, I., Peischl, J., Neuman, J.A., Brown, S.S., Thompson, C.R., Aikin, K.C., Allen, H.M.,
658 Angot, H., Apel, E.C., Baublitz, C.B. and Brewer, J.F., 2021. Large contribution of biomass
659 burning emissions to ozone throughout the global remote troposphere. Proceedings of the National
660 Academy of Sciences, 118(52), p.e2109628118.
661
662 Center for International Earth Science Information Network (CIESIN), Columbia University.
663 2018. Documentation for the Gridded Population of the World, Version 4 (GPWv4), Revision 11
664 Data Sets. Palisades NY: NASA Socioeconomic Data and Applications Center (SEDAC).
665 https://doi.org/10.7927/H45Q4T5F Accessed 2022-11-17.

666 Chin, M., Ginoux, P., Kinne, S., Torres, O., Holben, B.N., Duncan, B.N., Martin, R.V., Logan,
667 J.A., Higurashi, A., Nakajima, T., 2002. Tropospheric aerosol optical thickness from the GOCART
668 model and comparisons with satellite and sun photometer measurements. J. Atmos. Sci. 59, 461–
669 483. https://doi.org/10.1175/ 1520-0469(2002)059<0461:TAOTFT>2.0.CO;2.

670 Clarke, K., Ash, K., Coker, E.S., Sabo-Attwood, T. and Bainomugisha, E., 2022. A Social
671 Vulnerability Index for Air Pollution and Its Spatially Varying Relationship to PM2. 5 in Uganda.
672 Atmosphere, 13(8), p.1169.

https://doi.org/10.5194/gmd-2023-50
Preprint. Discussion started: 4 May 2023
© Author(s) 2023. CC BY 4.0 License.

673 Compernolle, S., Verhoelst, T., Pinardi, G., Granville, J., Hubert, D., Keppens, A., Niemeijer, S.,
674 Rino, B., Bais, A., Beirle, S., Boersma, F., Burrows, J. P., De Smedt, I., Eskes, H., Goutail, F.,
675 Hendrick, F., Lorente, A., Pazmino, A., Piters, A., Peters, E., Pommereau, J.-P., Remmers, J.,
676 Richter, A., van Geffen, J., Van Roozendael, M., Wagner, T., and Lambert, J.-C.: Validation of
677 Aura-OMI QA4ECV NO_2 climate data records with ground-based DOAS networks: the role of
678 measurement and comparison uncertainties, Atmos. Chem. Phys., 20, 8017–8045,
679 https://doi.org/10.5194/acp-20-8017-2020, 2020.

680 Darmenov, A., & da Silva, A. (2013). The quick fire emissions dataset (QFED)–documentation of
681 versions 2.1, 2.2 and 2.4. NASA Technical Report Series on Global Modeling and Data
682 Assimilation, NASA TM-2013-104606, 32, 183.

683 De Longueville, F., Hountondji, Y.C., Henry, S. and Ozer, P., 2010. What do we know about
684 effects of desert dust on air quality and human health in West Africa compared to other regions?.
685 Science of the total environment, 409(1), pp.1-8.

686 De Smedt, I., Yu, H., Richter, A., Beirle, S., Eskes, H., Boersma, K.F., Van Roozendael, M., Van
687 Geffen, J., Lorente, A. and Peters, E., (2017a), QA4ECV HCHO tropospheric column data from
688 OMI (Version 1.1). Royal Belgian Institute for Space Aeronomy.
689 http://doi.org/10.18758/71021031.

690 De Smedt, I., Van Geffen, J., Richter, A., Beirle S., Yu, H., Vlietinck J., Van Roozendael, M. van
691 der A R., Lorente A., Scanlon T., Compernolle S., Wagner T., Boersma, K. F., Eskes, H., 2017b,
692 Product User Guide for HCHO.

693 Deeter, M.N., 2009. MOPITT (Measurements of Pollution in the Troposphere) Validated Version
694 4 Product User's Guide. National Centre for Atmospheric Research, Boulder, CO, 80307.

695 Deeter, M. N.,Worden, H. M., Gille, J. C., Edwards, D. P.,Mao, D., and Drummond, J. R.:
696 MOPITT multispectral CO retrievals: Origins and effects of geophysical radiance errors, J.
697 Geophys. Res., 116, D15303, https://doi.org/10.1029/2011JD015703, 2011.

698 Deeter, M., Francis, G., Gille, J., Mao, D., Martínez-Alonso, S., Worden, H., Ziskin, D.,
699 Drummond, J., Commane, R., Diskin, G., and McKain, K.: The MOPITT Version 9 CO product:
700 sampling enhancements and validation, Atmos. Meas. Tech., 15, 2325–2344,
701 https://doi.org/10.5194/amt-15-2325-2022, 2022.

702 Emmons, L.K., Walters, S., Hess, P.G., Lamarque, J.-F., Pfister, G.G., Fillmore, D., Granier, C.,
703 Guenther, A., Kinnison, D., Laepple, T., Orlando, J., Tie, X., Tyndall, G., Wiedinmyer, C.,
704 Baughcum, S.L., Kloster, S., 2010. Description and evaluation of the model for ozone and related
705 chemical tracers, version 4 (MOZART-4). Geosci. Model Dev. 3, 43–67.
706 https://doi.org/10.5194/gmd-3-43-2010.

707 Emmons, L.K., Schwantes, R. H., Orlando, J. J., Tyndall, G., Kinnison, D., Lamarque, J.-F., et al.:
708 The Chemistry Mechanism in the Community Earth System Model version 2 (CESM2), Journal
709 of Advances in Modeling Earth Systems, 12, https://doi.org/10.1029/2019MS001882, 2020.

https://doi.org/10.5194/gmd-2023-50
Preprint. Discussion started: 4 May 2023
© Author(s) 2023. CC BY 4.0 License.

710 Fisher, J. A., Murray, L. T., Jones, D. B. A., & Deutscher, N. M. (2017). Improved method for
711 linear carbon monoxide simulation and source attribution in atmospheric chemistry models
712 illustrated using GEOS-Chem v9. Geoscientific Model Development, 10, 4129–4144.
713 https://doi.org/10.5194/gmd-10-4129-2017.

714 Fisher, S., Bellinger, D.C., Cropper, M.L., Kumar, P., Binagwaho, A., Koudenoukpo, J.B., Park,
715 Y., Taghian, G. and Landrigan, P.J., 2021. Air pollution and development in Africa: impacts on
716 health, the economy, and human capital. The Lancet Planetary Health, 5(10), pp.e681-e688.

717 Friedl, M., D. Sulla-Menashe. MODIS/Terra+Aqua Land Cover Type Yearly L3 Global 0.05Deg
718 CMG V061. 2022, distributed by NASA EOSDIS Land Processes DAAC,
719 https://doi.org/10.5067/MODIS/MCD12C1.061. Accessed 2022-11-17.

720 Gaubert, B., Arellano, A. F., Barré, J., Worden, H. M., Emmons, L. K., Tilmes, S., Buchholz, R.
721 R., Vitt, F., Raeder, K., Collins, N., Anderson, J. L., Wiedinmyer, C., Martínez-Alonso, S.,
722 Edwards, D. P., Andreae, M. O., Hannigan, J. W., Petri, C., Strong, K., and Jones, N.: Toward a
723 chemical reanalysis in a coupled chemistry-climate model: An evaluation of MOPITT CO
724 assimilation and its impact on tropospheric composition, J. Geophys. Res.-Atmos., 121, 7310–
725 7343, https://doi.org/10.1002/2016JD024863, 2016.

726 Gaubert, B., Emmons, L. K., Raeder, K., Tilmes, S., Miyazaki, K., Arellano Jr., A. F., Elguindi,
727 N., Granier, C., Tang, W., Barré, J., Worden, H. M., Buchholz, R. R., Edwards, D. P., Franke, P.,
728 Anderson, J. L., Saunois, M., Schroeder, J., Woo, J.-H., Simpson, I. J., Blake, D. R., Meinardi, S.,
729 Wennberg, P. O., Crounse, J., Teng, A., Kim, M., Dickerson, R. R., He, H., Ren, X., Pusede, S. E.,
730 and Diskin, G. S.: Correcting model biases of CO in East Asia: impact on oxidant distributions
731 during KORUS-AQ, Atmos. Chem. Phys., 20, 14617–14647, https://doi.org/10.5194/acp-20-
732 14617-2020, 2020.

733 Gelaro, R., McCarty, W., Suárez, M. J., Todling, R., Molod, A., Takacs, L., et al. (2017). The
734 modern-era retrospective analysis for research and applications, version 2 (MERRA-2). Journal of
735 Climate, 30(14), 5419-5454.

736 Güneralp, B., Lwasa, S., Masundire, H., Parnell, S. and Seto, K.C., 2017. Urbanization in Africa:
737 challenges and opportunities for conservation. Environmental research letters, 13(1), p.015002.

738 Heft-Neal, S., Burney, J., Bendavid, E. and Burke, M., 2018. Robust relationship between air
739 quality and infant mortality in Africa. Nature, 559(7713), pp.254-258.

740 Hsu, N.C., Jeong, M.J., Bettenhausen, C., Sayer, A.M., Hansell, R., Seftor, C.S., Huang, J. and
741 Tsay, S.C., 2013. Enhanced Deep Blue aerosol retrieval algorithm: The second generation. Journal
742 of Geophysical Research: Atmospheres, 118(16), pp.9296-9315.

743 Jo, D., et al., Effects of Grid Resolution and Emission Inventory on Urban Air Quality Simulation
744 With the Multi-Scale Infrastructure for Chemistry and Aerosols (MUSICA) Version 0, JAMES,
745 in review, 2022.

746 Kuik, F., Lauer, A., Beukes, J. P., Van Zyl, P. G., Josipovic, M., Vakkari, V., Laakso, L., and Feig,
747 G. T.: The anthropogenic contribution to atmospheric black carbon concentrations in southern

https://doi.org/10.5194/gmd-2023-50
Preprint. Discussion started: 4 May 2023
© Author(s) 2023. CC BY 4.0 License.

748 Africa: a WRF-Chem modeling study, Atmos. Chem. Phys., 15, 8809–8830,
749 https://doi.org/10.5194/acp-15-8809-2015, 2015.

750 Kumar, R., He, C., Bhardwaj, P., Lacey, F., Buchholz, R.R., Brasseur, G.P., Joubert, W.,
751 Labuschagne, C., Kozlova, E. and Mkololo, T., 2022. Assessment of regional carbon monoxide
752 simulations over Africa and insights into source attribution and regional transport. Atmospheric
753 Environment, 277, p.119075.

754 Lacey, F. G., Marais, E. A., Henze, D. K., Lee, C. J., van Donkelaar, A., Martin, R. V., et al. (2017).
755 Improving present day and future estimates of anthropogenic sectoral emissions and the resulting
756 air quality impacts in Africa. Faraday Discussions, 200, 397–412.
757 https://doi.org/10.1039/C7FD00011A.

758 Lauritzen, P. H., Nair, R. D., Herrington, A. R., Callaghan, P., Goldhaber, S., Dennis, J. M.,
759 Bacmeister, J. T., Eaton, B. E., Zarzycki, C. M., Taylor, M. A., Ullrich, P. A., Dubos, T., Gettelman,
760 A., Neale, R. B., Dobbins, B., Reed, K. A., Hannay, C., Medeiros, B., Benedict, J. J. and Tribbia,
761 J. J.: NCAR Release of CAM-SE in CESM2.0: A Reformulation of the Spectral Element
762 Dynamical Core in Dry-Mass Vertical Coordinates With Comprehensive Treatment of
763 Condensates and Energy, Journal of Advances in Modeling Earth Systems, 10(7), 1537–1570,
764 2018.

765 Levy, R. C., Mattoo, S., Munchak, L. A., Remer, L. A., Sayer, A. M., Patadia, F., and Hsu, N. C.:
766 The Collection 6 MODIS aerosol products over land and ocean, Atmos. Meas. Tech., 6, 2989–
767 3034, https://doi.org/10.5194/amt-6-2989-2013, 2013.

768 Levy, R., Hsu, C., et al., 2017. MODIS Atmosphere L2 Aerosol Product. NASA MODIS Adaptive
769 Processing System, Goddard Space Flight Center, USA:
770 http://dx.doi.org/10.5067/MODIS/MOD04_L2.061.

771 Liousse, C., Assamoi, E., Criqui, P., Granier, C., and Rosset, R.: Explosive growth in African
772 combustion emissions from 2005 to 2030, Environ. Res. Lett., 9, 35003,
773 https://doi.org/10.1088/1748-9326/9/3/035003, 2014.

774 Liu, J. C., Mickley, L. J., Sulprizio, M. P., Dominici, F., Yue, X., Ebisu, K., ... & Bell, M. L. (2016).
775 Particulate air pollution from wildfires in the Western US under climate change. Climatic change,
776 138(3), 655-666.

777 Malings, C., Westervelt, D. M., Hauryliuk, A., Presto, A. A., Grieshop, A., Bittner, A., Beekmann,
778 M., and R. Subramanian: Application of low-cost fine particulate mass monitors to convert satellite
779 aerosol optical depth to surface concentrations in North America and Africa, Atmos. Meas. Tech.,
780 13, 3873–3892, https://doi.org/10.5194/amt-13-3873-2020, 2020.

781 Marais, E. A., Jacob, D. J., Kurosu, T. P., Chance, K., Murphy, J. G., Reeves, C., Mills, G., Casadio,
782 S., Millet, D. B., Barkley, M. P., Paulot, F., and Mao, J.: Isoprene emissions in Africa inferred
783 from OMI observations of formaldehyde columns, Atmos. Chem. Phys., 12, 6219–6235,
784 https://doi.org/10.5194/acp-12-6219-2012, 2012.

https://doi.org/10.5194/gmd-2023-50
Preprint. Discussion started: 4 May 2023
© Author(s) 2023. CC BY 4.0 License.

785 Marais, E.A., Silvern, R.F., Vodonos, A., Dupin, E., Bockarie, A.S., Mickley, L.J. and Schwartz,
786 J., 2019. Air quality and health impact of future fossil fuel use for electricity generation and
787 transport in Africa. Environmental science & technology, 53(22), pp.13524-13534.

788 Mazzeo, A., Burrow, M., Quinn, A., Marais, E. A., Singh, A., Ng'ang'a, D., Gatari, M. J., and Pope,
789 F. D.: Evaluation of the WRF and CHIMERE models for the simulation of PM2.5 in large East
790 African urban conurbations, Atmos. Chem. Phys., 22, 10677–10701, https://doi.org/10.5194/acp-
791 22-10677-2022, 2022.

792 Menut, L., Flamant, C., Turquety, S., Deroubaix, A., Chazette, P., and Meynadier, R.: Impact of
793 biomass burning on pollutant surface concentrations in megacities of the Gulf of Guinea, Atmos.
794 Chem. Phys., 18, 2687–2707, https://doi.org/10.5194/acp-18-2687-2018, 2018.

795 Nicholson, S.E., 2019. A review of climate dynamics and climate variability in Eastern Africa.
796 The limnology, climatology and paleoclimatology of the East African lakes, pp.25-56.

797 Paton-Walsh, C., Emmerson, K.M., Garland, R.M., Keywood, M., Hoelzemann, J.J., Huneeus, N.,
798 Buchholz, R.R., Humphries, R.S., Altieri, K., Schmale, J. and Wilson, S.R., 2022. Key challenges
799 for tropospheric chemistry in the Southern Hemisphere. Elem Sci Anth, 10(1), p.00050.

800 Petkova, E.P., Jack, D.W., Volavka-Close, N.H. and Kinney, P.L., 2013. Particulate matter
801 pollution in African cities. Air Quality, Atmosphere & Health, 6(3), pp.603-614.

802 Petzold, A., Thouret, V., Gerbig, C., Zahn, A., Brenninkmeijer, C.A., Gallagher, M., Hermann,
803 M., Pontaud, M., Ziereis, H., Boulanger, D. and Marshall, J., 2015. Global-scale atmosphere
804 monitoring by in-service aircraft–current achievements and future prospects of the European
805 Research Infrastructure IAGOS. Tellus B: Chemical and Physical Meteorology, 67(1), p.28452.

806 Pfister, G. G., Eastham, S. D., Arellano, A. F., Aumont, B., Barsanti, K. C., Barth, M. C., ... &
807 Brasseur, G. P. (2020). The Multi-Scale Infrastructure for Chemistry and Aerosols (MUSICA).
808 Bulletin of the American Meteorological Society, 101(10), E1743-E1760.

809 Schwantes, R.H., Lacey, F.G., Tilmes, S., Emmons, L.K., Lauritzen, P.H., Walters, S., Callaghan,
810 P., Zarzycki, C.M., Barth, M.C., Jo, D.S. and Bacmeister, J.T., 2022. Evaluating the impact of
811 chemical complexity and horizontal resolution on tropospheric ozone over the conterminous US
812 with a global variable resolution chemistry model. Journal of Advances in Modeling Earth Systems,
813 14(6), p.e2021MS002889.

814 Shindell, D. T., Faluvegi, G., Stevenson, D. S., Krol, M. C., Emmons, L. K., Lamarque, J. F., et
815 al. (2006). Multimodel simulations of carbon monoxide: Comparison with observations and
816 projected near-future changes. Journal of Geophysical Research, 111.

817 Soulie, A., C. Granier, S. Darras, T. Doumbia, M. Guevara, J.-P. Jalkanen, S. Keita, C. Liousse,
818 Global anthropogenic emissions (CAMS-GLOB-ANT) for the Copernicus Atmosphere
819 Monitoring Service Air Quality Forecasts and Reanalysis, to be submitted to Earth Sys. Sci. data,
820 2023.

https://doi.org/10.5194/gmd-2023-50
Preprint. Discussion started: 4 May 2023
© Author(s) 2023. CC BY 4.0 License.

821 Stauffer, R.M., Thompson, A.M., Kollonige, D.E., Witte, J.C., Tarasick, D.W., Davies, J., Vömel,
822 H., Morris, G.A., Van Malderen, R., Johnson, B.J. and Querel, R.R., 2020. A post-2013 dropoff
823 in total ozone at a third of global ozonesonde stations: Electrochemical concentration cell
824 instrument artifacts?. Geophysical Research Letters, 47(11), p.e2019GL086791.

825 Stein, O., Schultz, M. G., Bouarar, I., Clark, H., Huijnen, V., Gaudel, A., et al. (2014). On the
826 wintertime low bias of Northern Hemisphere carbon monoxide found in global model simulations.
827 Atmospheric Chemistry and Physics, 14, 9295–9316.

828 Tang, W., Arellano, A. F., DiGangi, J. P., Choi, Y., Diskin, G. S., Agustí-Panareda, A., Parrington,
829 M., Massart, S., Gaubert, B., Lee, Y., Kim, D., Jung, J., Hong, J., Hong, J.-W., Kanaya, Y., Lee,
830 M., Stauffer, R. M., Thompson, A. M., Flynn, J. H., and Woo, J.-H.: Evaluating high-resolution
831 forecasts of atmospheric CO and CO2 from a global prediction system during KORUS-AQ field
832 campaign, Atmos. Chem. Phys., 18, 11007–11030, https://doi.org/10.5194/acp-18-11007-2018,
833 2018.

834 Tang, W., Emmons, L. K., Arellano Jr., A. F., Gaubert, B., Knote, C., Tilmes, S., Buchholz, R. R.,
835 Pfister, G. G., Diskin, G. S., Blake, D. R., Blake, N. J., Meinardi, S., DiGangi, J. P., Choi, Y., Woo,
836 J.-H., He, C., Schroeder, J. R., Suh, I., Lee, H.-J., Jo, H.-Y., Kanaya, Y., Jung, J., Lee, Y., and Kim,
837 D.: Source contributions to carbon monoxide concentrations during KORUS-AQ based on CAM-
838 chem model applications, J. Geophys. Res.-Atmos., 124, 1–27,
839 https://doi.org/10.1029/2018jd029151, 2019.

840 Tang, W., Emmons, L.K., Buchholz, R.R., Wiedinmyer, C., Schwantes, R.H., He, C., Kumar, R.,
841 Pfister, G.G., Worden, H.M., Hornbrook, R.S. and Apel, E.C., 2022. Effects of Fire Diurnal
842 Variation and Plume Rise on US Air Quality During FIREX-AQ and WE-CAN Based on the
843 Multi-Scale Infrastructure for Chemistry and Aerosols (MUSICAv0). Journal of Geophysical
844 Research: Atmospheres, 127(16), p.e2022JD036650.

845 Taylor, K. E. (2001). Summarizing multiple aspects of model performance in a single diagram.
846 Journal of Geophysical Research, 106(1755), 7183–7192. https://doi.org/10.1029/2000JD900719.

847 Thompson, A. M., Balashov, N. V., Witte, J. C., Coetzee, J. G. R., Thouret, V., and Posny, F.:
848 Tropospheric ozone increases over the southern Africa region: bellwether for rapid growth in
849 Southern Hemisphere pollution?, Atmos. Chem. Phys., 14, 9855–9869,
850 https://doi.org/10.5194/acp-14-9855-2014, 2014.

851 Thompson, A. M., J. C. Witte, C., Sterling, A., Jordan, B. J., Johnson, S. J. Oltmans, ... Thiongo,
852 K. (2017). First reprocessing of Southern Hemisphere Additional Ozonesondes (SHADOZ) ozone
853 profiles (1998-2016): 2. Comparisons with satellites and ground-based instruments. Journal of
854 Geophysical Research: Atmospheres, 122, 13,000-13,025. https://doi.org/10.1002/2017JD027406.

855 Thompson, C. R., Wofsy, S. C., Prather, M. J., Newman, P. A., Hanisco, T. F., Ryerson, T. B.,
856 Fahey, D. W., Apel, E. C., Brock, C. A., Brune, W. H., Froyd, K., Katich, J. M., Nicely, J. M.,
857 Peischl, J., Ray, E., Veres, P. R., Wang, S., Allen, H. M., Asher, E., Bian, H., Blake, D., Bourgeois,
858 I., Budney, J., Bui, T. P., Butler, A., Campuzano-Jost, P., Chang, C., Chin, M., Commane, R.,
859 Correa, G., Crounse, J. D., Daube, B., Dibb, J. E., DiGangi, J. P., Diskin, G. S., Dollner, M., Elkins,
860 J. W., Fiore, A. M., Flynn, C. M., Guo, H., Hall, S. R., Hannun, R. A., Hills, A., Hintsa, E. J.,

https://doi.org/10.5194/gmd-2023-50
Preprint. Discussion started: 4 May 2023
© Author(s) 2023. CC BY 4.0 License.

Hodzic, A., Hornbrook, R. S., Huey, L. G., Jimenez, J. L., Keeling, R. F., Kim, M. J., Kupc, A., Lacey, F., Lait, L. R., Lamarque, J., Liu, J., McKain, K., Meinardi, S., Miller, D. O., Montzka, S. A., Moore, F. L., Morgan, E. J., Murphy, D. M., Murray, L. T., Nault, B. A., Neuman, J. A., Nguyen, L., Gonzalez, Y., Rollins, A., Rosenlof, K., Sargent, M., Schill, G., Schwarz, J. P., Clair, J. M. S., Steenrod, S. D., Stephens, B. B., Strahan, S. E., Strode, S. A., Sweeney, C., Thames, A. B., Ullmann, K., Wagner, N., Weber, R., Weinzierl, B., Wennberg, P. O., Williamson, C. J., Wolfe, G. M., and Zeng, L.: The NASA Atmospheric Tomography (ATom) Mission: Imaging the Chemistry of the Global Atmosphere, B. Am. Meteorol. Soc., 103, E761–E790, 2022.

Tilmes, S., Lamarque, J. F., Emmons, L. K., Kinnison, D. E., Ma, P. L., Liu, X., et al. (2015). Description and evaluation of tropospheric chemistry and aerosols in the Community Earth System Model (CESM1. 2). Geoscientific Model Development, 8, 1395–1426.

Tilmes, S., Hodzic, A., Emmons, L. K., Mills, M. J., Gettelman, A., Kinnison, D. E., et al.: Climate forcing and trends of organic aerosols in the Community Earth System Model (CESM2). Journal of Advances in Modeling Earth Systems, 11, https://doi.org/10.1029/2019MS001827, 2019.

U.S. EPA: Quality Assurance Guidance Document 2.12: Monitoring PM2.5 in Ambient Air Using Designated Reference or Class I Equivalent Methods, United States Environmental Protection Agency, available at: https://www3.epa.gov/ttnamti1/files/ambient/pm25/qa/m212.pdf (last access: 20 November 2022), 2016.

van der Werf, G. R., Randerson, J. T., Giglio, L., van Leeuwen, T. T., Chen, Y., Rogers, B. M., Mu, M., van Marle, M. J. E., Morton, D. C., Collatz, G. J., Yokelson, R. J., and Kasibhatla, P. S., 2017. Global fire emissions estimates during 1997–2016, Earth Syst. Sci. Data, 9, 697–720, https://doi.org/10.5194/essd-9-697-2017.

Vohra, K., Marais, E.A., Bloss, W.J., Schwartz, J., Mickley, L.J., Van Damme, M., Clarisse, L. and Coheur, P.F., 2022. Rapid rise in premature mortality due to anthropogenic air pollution in fast-growing tropical cities from 2005 to 2018. Science Advances, 8(14), p.eabm4435.

Washington, R., Harrison, M., Conway, D., Black, E., Challinor, A., Grimes, D., Jones, R., Morse, A., Kay, G. and Todd, M., 2006. African climate change: taking the shorter route. Bulletin of the American Meteorological Society, 87(10), pp.1355-1366.

Watson, J. G., Chow, J. C., Moosmüller, H., Green, M., Frank, N., and Pitchford, M.: Guidance for using continuous monitors in PM2.5 monitoring networks, U.S. EPA Office of Air Quality Planning and Standards, Triangle Park, NC., 1998.

Wiedinmyer, C., Akagi, S.K., Yokelson, R.J., Emmons, L.K., Al-Saadi, J.A., Orlando, J.J., Soja, A.J., 2011. The Fire INventory from NCAR (FINN): a high resolution global model to estimate the emissions from open burning. Geosci. Model Dev. 4, 625–641. https://doi.org/10.5194/gmd-4-625-2011.

Wiedinmyer, C., Yokelson, R. J., and Gullett, B. K.: Global emissions of trace gases, particulate matter, and hazardous air pollutants from open burning of domestic waste, Environ. Sci. Technol., 48, 9523–9530, https://doi.org/10.1021/es502250z, 2014.

https://doi.org/10.5194/gmd-2023-50
Preprint. Discussion started: 4 May 2023
© Author(s) 2023. CC BY 4.0 License.

Geoscientific Model Development Discussions
Open Access
EGU

899 Witte, J.C., A. M. Thompson, H. G. J. Smit, M. Fujiwara, F. Posny, Gert J. R. Coetzee, ... F. R. da
900 Silva (2017), First reprocessing of Southern Hemisphere ADditional OZonesondes (SHADOZ)
901 profile records (1998-2015): 1. Methodology and evaluation, J. Geophys. Res. Atmos., 122, 6611-
902 6636. https://doi.org/10.1002/2016JD026403.

903 Witte, J. C., Thompson, A. M., Smit, H. G. J., Vömel, H., Posny, F., & Stübi, R. (2018). First
904 reprocessing of Southern Hemisphere ADditional OZonesondes profile records: 3. Uncertainty in
905 ozone profile and total column. Journal of Geophysical Research: Atmospheres, 123, 3243-3268.
906 https://doi.org/10.1002/2017JD027791.

907 Worden, H. M., Deeter, M. N., Edwards, D. P., Gille, J. C., Drummond, J. R., and Nédélec, P.:
908 Observations of near-surface carbon monoxide from space using MOPITT multispectral retrievals,
909 J. Geophys. Res., 115, D18314, https://doi.org/10.1029/2010JD014242, 2010.

910 Ziervogel, G., New, M., Archer van Garderen, E., Midgley, G., Taylor, A., Hamann, R., Stuart-
911 Hill, S., Myers, J. and Warburton, M., 2014. Climate change impacts and adaptation in South
912 Africa. Wiley Interdisciplinary Reviews: Climate Change, 5(5), pp.605-620.

913

914

915

916

917
918
919
920
921

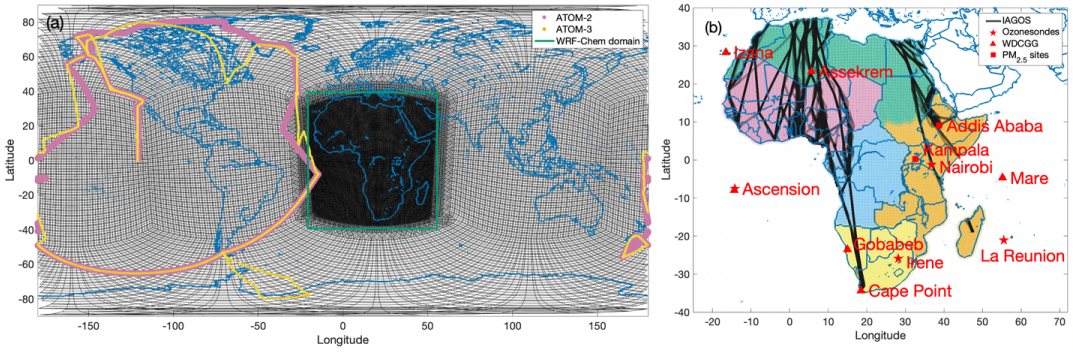

922
923 **Figure 1.** Model grid, in situ observations used in this study, and sub-regions in Africa. (a)
924 MUSICAv0 model grid developed for Africa in this study (black), domain boundary of the WRF-
925 Chem simulation compared in this study (shown by green box), observations from the
926 Atmospheric Tomography Mission (ATom) field campaign 2 (ATom-2; 2017 Jan to 2017 Feb;
927 pink) and ATom-3 (2017 Sep to 2017 Oct; yellow). (b) Sub-regions in Africa are shown, namely

https://doi.org/10.5194/gmd-2023-50
Preprint. Discussion started: 4 May 2023
© Author(s) 2023. CC BY 4.0 License.

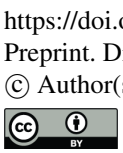

Geoscientific Model Development Discussions
Open Access
EGU

North Africa (green), West Africa (pink), East Africa (orange), Central Africa (blue), and Southern Africa (yellow). Location of in situ observations are labeled on the map. Flight tracks of the In-service Aircraft for a Global Observing System (IAGOS) are shown with black lines. Four ozonesonde sites are shown by pentagrams (Ascension, Irene, Nairobi, and La Reunion); six sites from the World Data Centre for Greenhouse Gases are shown by triangles (Assekrem, Cape Point, Izana, Gobabeb, Mare, and Ascension); two surface sites for $PM_{2.5}$ are shown by squares (Addis Ababa and Kampala).

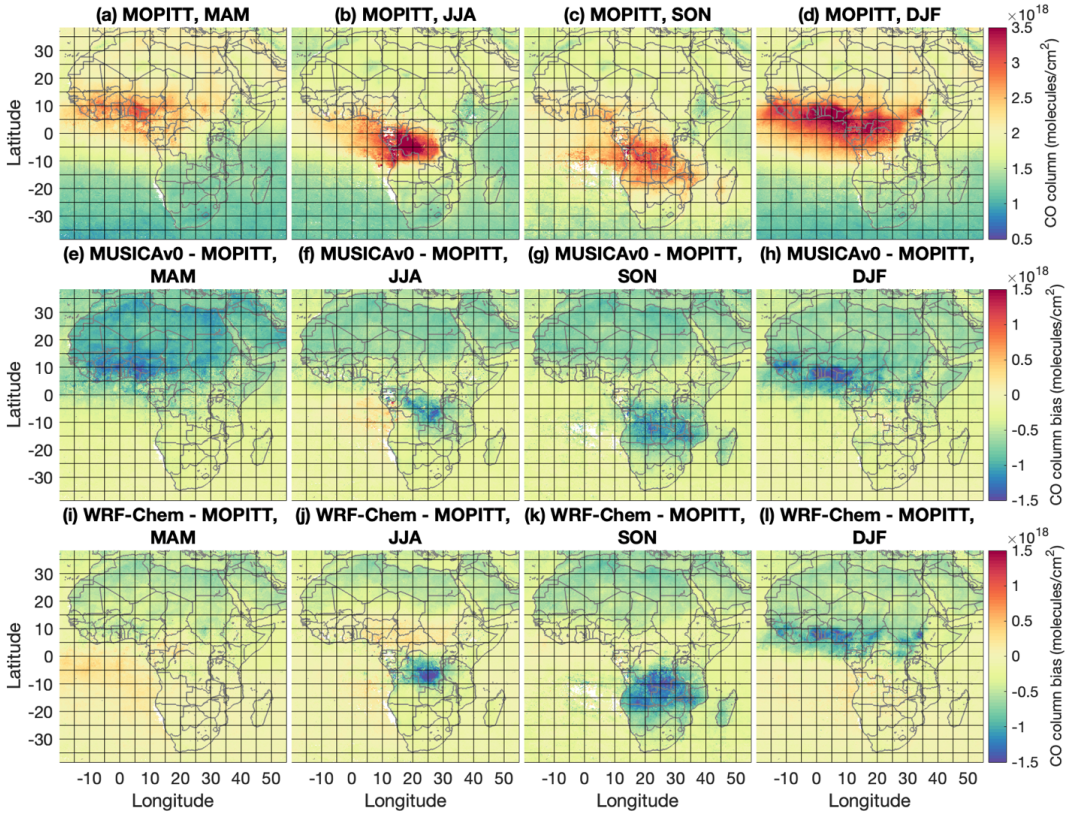

Figure 2. Comparisons of MUSICAv0 and WRF-Chem simulations to MOPITT CO column (molecules/cm^2) for each season of 2017. (a-d) Averaged MOPITT CO column: MAM (March, April, and May), JJA (June, July, and August), SON (September, October, and November), and DJF (December, January, and February). (e-h) MUSICAv0 model biases against MOPITT CO column for MAM, JJA, SON, and DJF. (i-l) is the same as (e-h) but for WRF-Chem. All data are gridded to 0.25 degree × 0.25 degree for plotting.

https://doi.org/10.5194/gmd-2023-50
Preprint. Discussion started: 4 May 2023
© Author(s) 2023. CC BY 4.0 License.

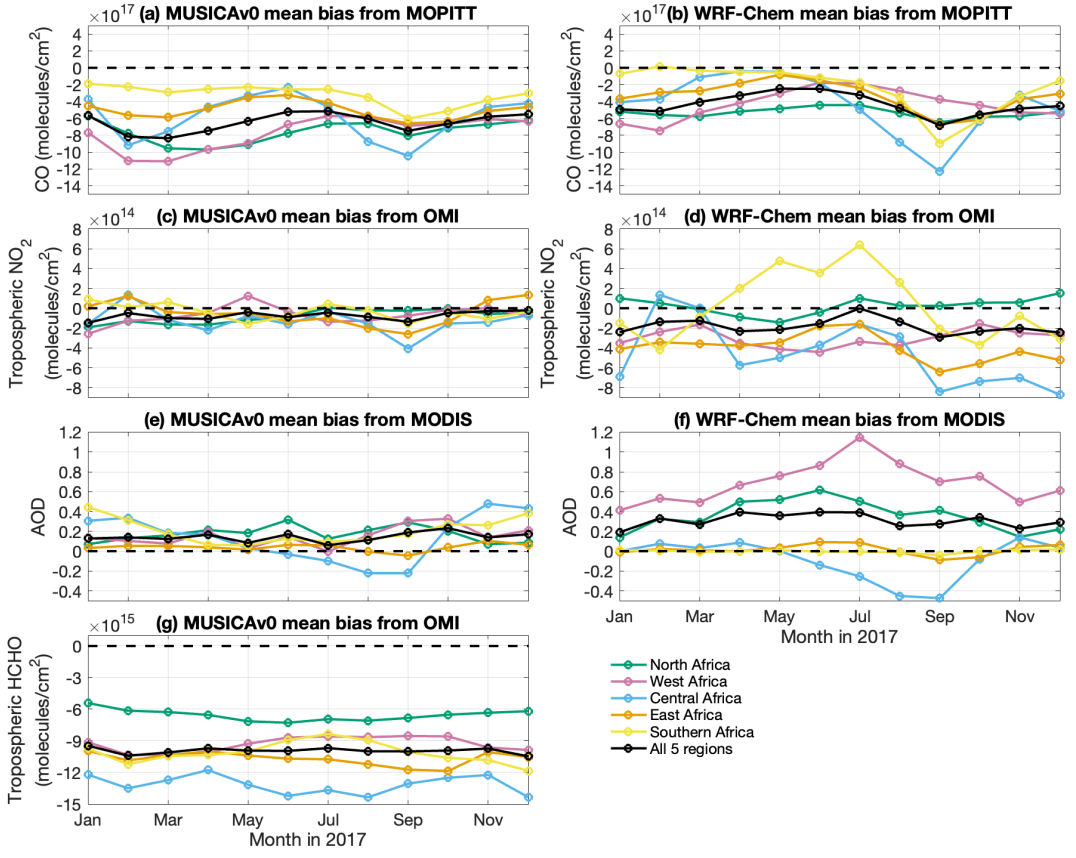

Figure 3. Mean bias of MUSICAv0 and WRF-Chem simulations from satellite data. Monthly timeseries of mean bias of (a) MUSICAv0 and (b) WRF-Chem against MOPITT CO column (molecules/cm^2) in 2017 over Africa (black), North Africa (green), West Africa (pink), East Africa (orange), Central Africa (blue), and Southern Africa (yellow). (c-d) are same as (a-b) but for mean bias against OMI tropospheric NO_2 column (molecules/cm^2). (e-f) are same as (a-b) but for mean bias against with MODIS (Terra) Aerosol Optical Depth (AOD). (g) is the same as (a) but for mean bias against OMI tropospheric HCHO column (molecules/cm^2).

https://doi.org/10.5194/gmd-2023-50
Preprint. Discussion started: 4 May 2023
© Author(s) 2023. CC BY 4.0 License.

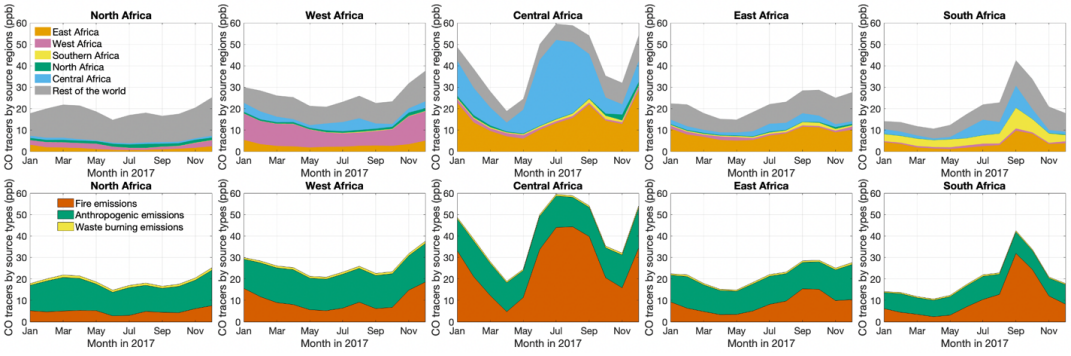

Figure 4. Monthly time series of column-averaged CO tracers in North Africa, West Africa, East Africa, Central Africa, and Southern Africa. Top panels show CO tracers of emissions from North Africa (green), West Africa (pink), East Africa (orange), Central Africa (blue), Southern Africa (yellow), and the rest of the world (grey). Bottom panels show CO tracers of fire emissions (red), anthropogenic emissions (green), and waste burning emissions (yellow).

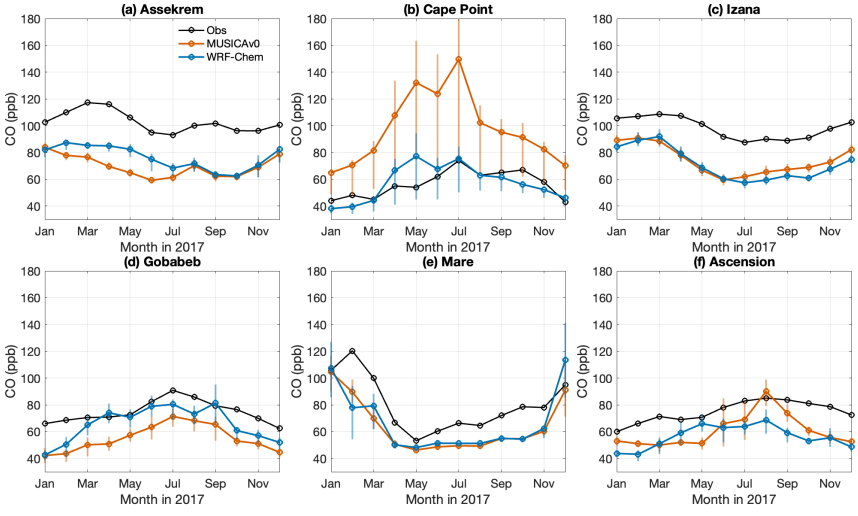

Figure 5. Monthly mean CO (ppb) from in situ observations (black), MUSICAv0 (red), and WRF-Chem (blue) during 2017 at (a) Assekrem, (b) Cape Point, (c) Izana, (d) Gobabeb, (e) Mare and (f) Ascension (see Figure 1b for locations). Monthly means are calculated from 3-hourly data. The range for each data point shows the variation of the 3-hourly data on that day (25% quantile to 75% quantile). Observational data are from World Data Centre for Greenhouse Gases (WDCGG).

https://doi.org/10.5194/gmd-2023-50
Preprint. Discussion started: 4 May 2023
© Author(s) 2023. CC BY 4.0 License.

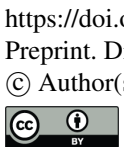

Geoscientific Model Development Discussions
Open Access
EGU

973
974

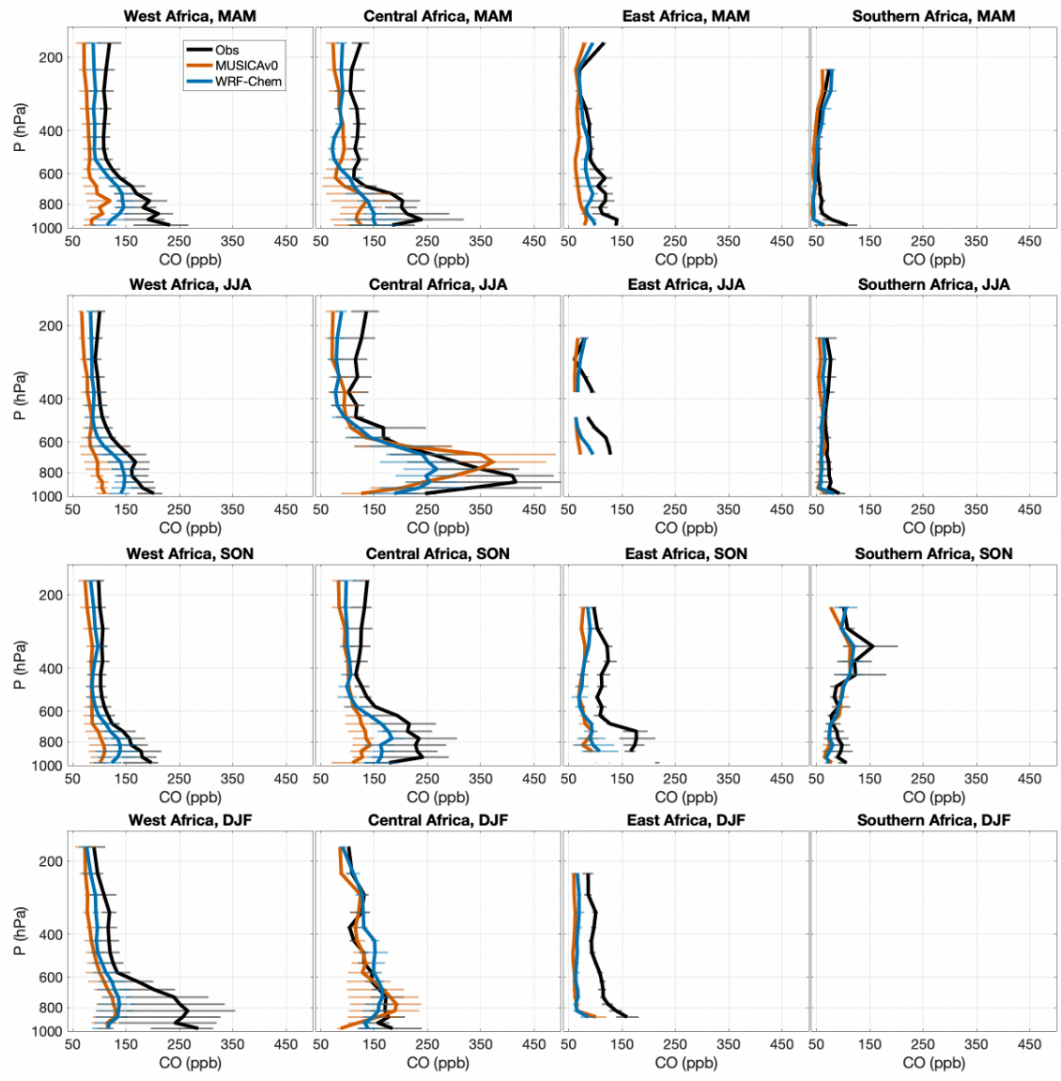

975
976 **Figure 6**. Vertical profiles of CO (ppb) from the In-service Aircraft for a Global Observing System
977 (IAGOS) measurements (black) and corresponding model output from MUSICAv0 (red), and
978 WRF-Chem (blue) during different seasons in 2017 over West Africa, Central Africa, East Africa,
979 and Southern Africa. North Africa is not shown due to data availability. Seasonal mean profiles
980 with the variation of the data in the pressure layer (25% quantile to 75% quantile) in MAM (March,
981 April, and May), JJA (June, July, and August), SON (September, October, and November), and
982 DJF (December, January, and February) are shown.
983

https://doi.org/10.5194/gmd-2023-50
Preprint. Discussion started: 4 May 2023
© Author(s) 2023. CC BY 4.0 License.

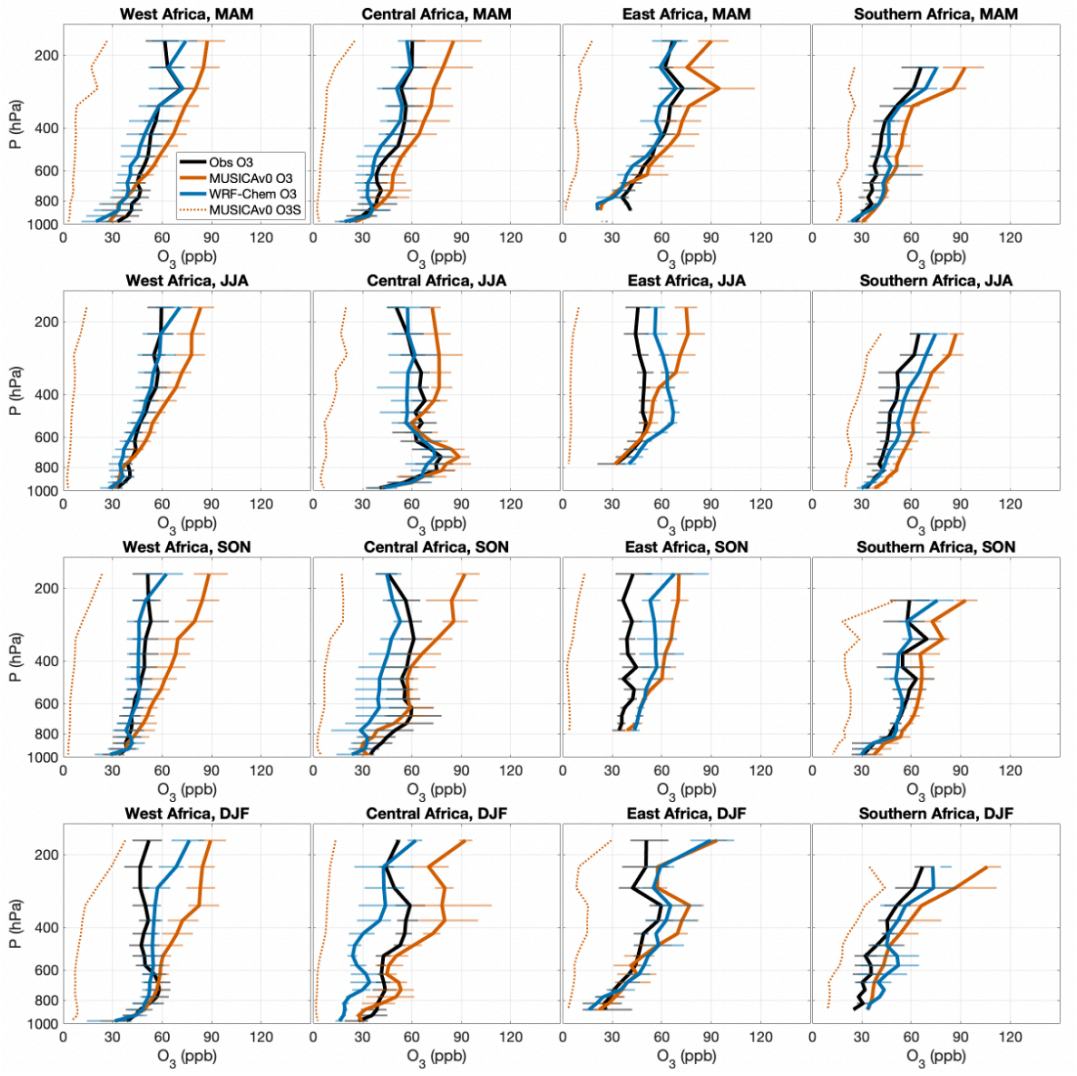

Figure 7. Vertical profiles of O_3 (ppb) from the In-service Aircraft for a Global Observing System (IAGOS) measurements (black) and corresponding model output from MUSICAv0 (red), and WRF-Chem (blue) during different seasons in 2017 over West Africa, Central Africa, East Africa, and Southern Africa. North Africa is not shown due to data availability Seasonal mean profiles with the variation of the data in the pressure layer (25% quantile to 75% quantile) in MAM (March, April, and May), JJA (June, July, and August), SON (September, October, and November), and DJF (December, January, and February) are shown. The dash red lines represent O3S (stratospheric ozone tracer) from the MUSICAv0 simulation.

https://doi.org/10.5194/gmd-2023-50
Preprint. Discussion started: 4 May 2023
© Author(s) 2023. CC BY 4.0 License.

Geoscientific Model Development
Discussions
Open Access
EGU

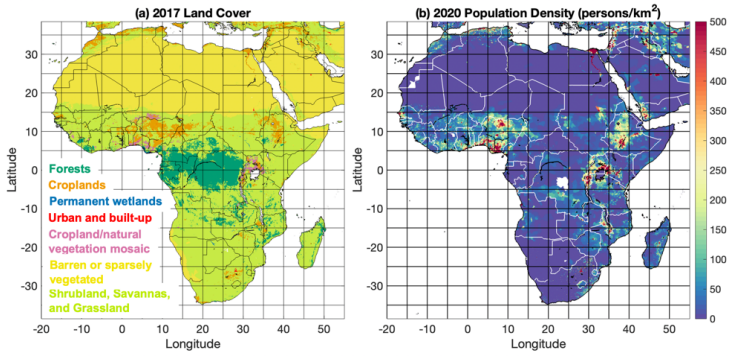

Figure 8. (a) Land cover in 2017 and (b) population density (persons/km^2) in 2020 over Africa. Land cover data is from MODIS/Terra+Aqua Land Cover Type Yearly L3 Global product (resolution: 0.05 degree) (Friedl et al., 2022). Cropland/Natural Vegetation Mosaics means Mosaics of small-scale cultivation (40-60%) with natural tree, shrub, or herbaceous vegetation. Population density data is from the Gridded Population of the World, Version 4 (GPWv4), Revision 11 (CIESIN, 2018).

https://doi.org/10.5194/gmd-2023-50
Preprint. Discussion started: 4 May 2023
© Author(s) 2023. CC BY 4.0 License.

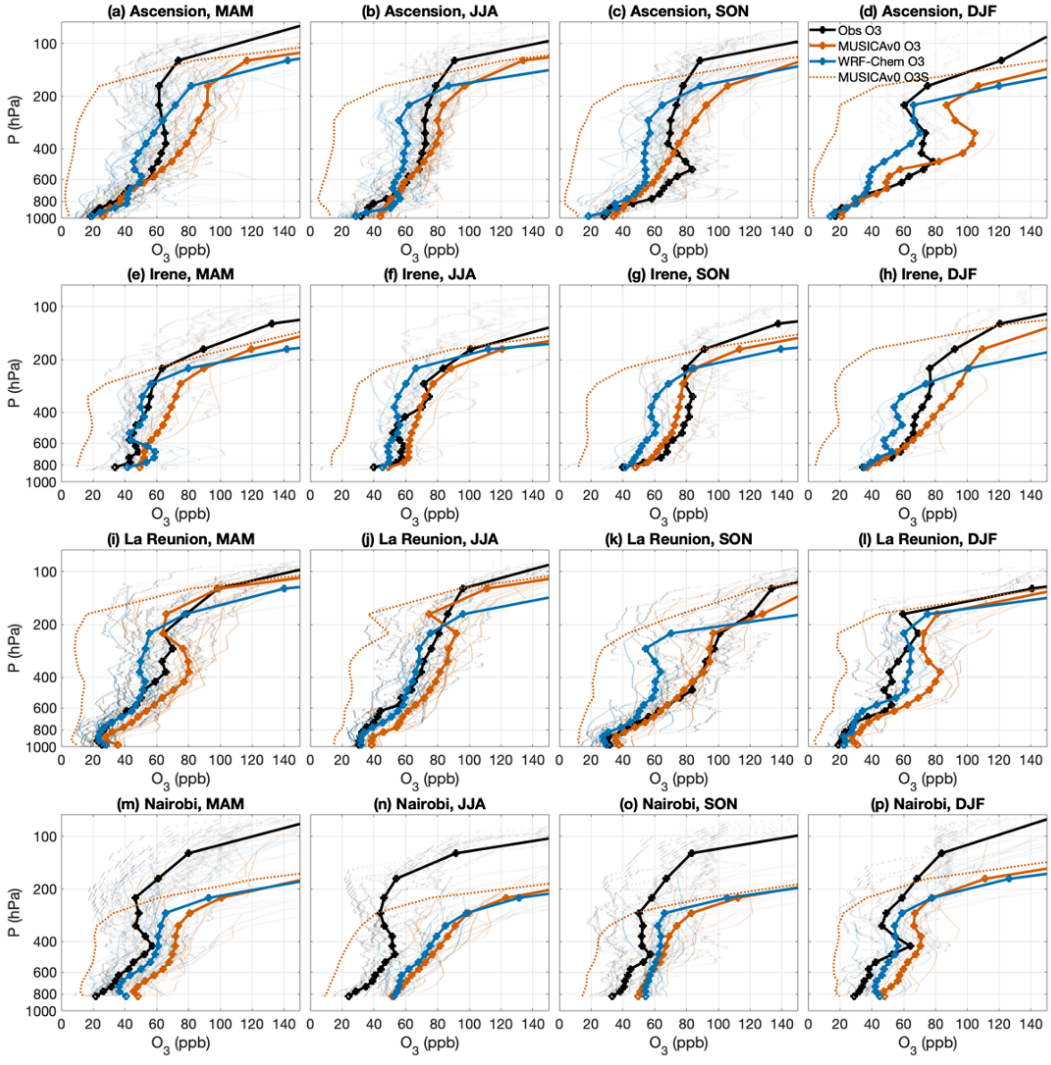

Figure 9. Vertical profiles of O_3 (ppb) from Ozonesondes (black) and corresponding model output from MUSICAv0 (red), and WRF-Chem (blue) for each season of 2017. The thick lines denote the seasonal mean profiles and the thin lines denote the individual profiles. The dash red lines represent O3S (stratospheric ozone tracer) from the MUSICAv0 simulation. Ozonesonde data at Ascension in (a) MAM (March, April, and May), (b) JJA (June, July, and August), (c) SON (September, October, and November), and (d) DJF (December, January, and February) are shown. (e-h), (i-l), and (m-p) are the same as (a-d), except for Irene, La Reunion, and Nairobi, respectively. Locations of the sites are shown in Figure 1b.

https://doi.org/10.5194/gmd-2023-50
Preprint. Discussion started: 4 May 2023
© Author(s) 2023. CC BY 4.0 License.

Geoscientific Model Development
Discussions
Open Access
EGU

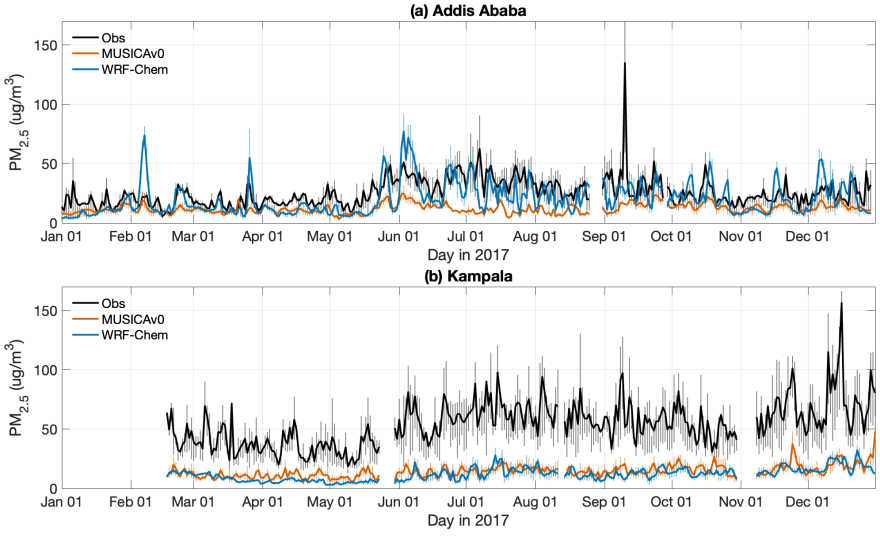

Figure 10. Daily mean $PM_{2.5}$ from in situ observations (black), MUSICAv0 (red), and WRF-Chem (blue) during 2017 at (a) Addis Ababa and (b) Kampala. Daily means are calculated from 3-hourly data. The shown range for each data point shows the variation on that day (25% quantile to 75% quantile). Locations of the sites are shown in Figure 1b.

https://doi.org/10.5194/gmd-2023-50
Preprint. Discussion started: 4 May 2023
© Author(s) 2023. CC BY 4.0 License.

Geoscientific Model Development Discussions

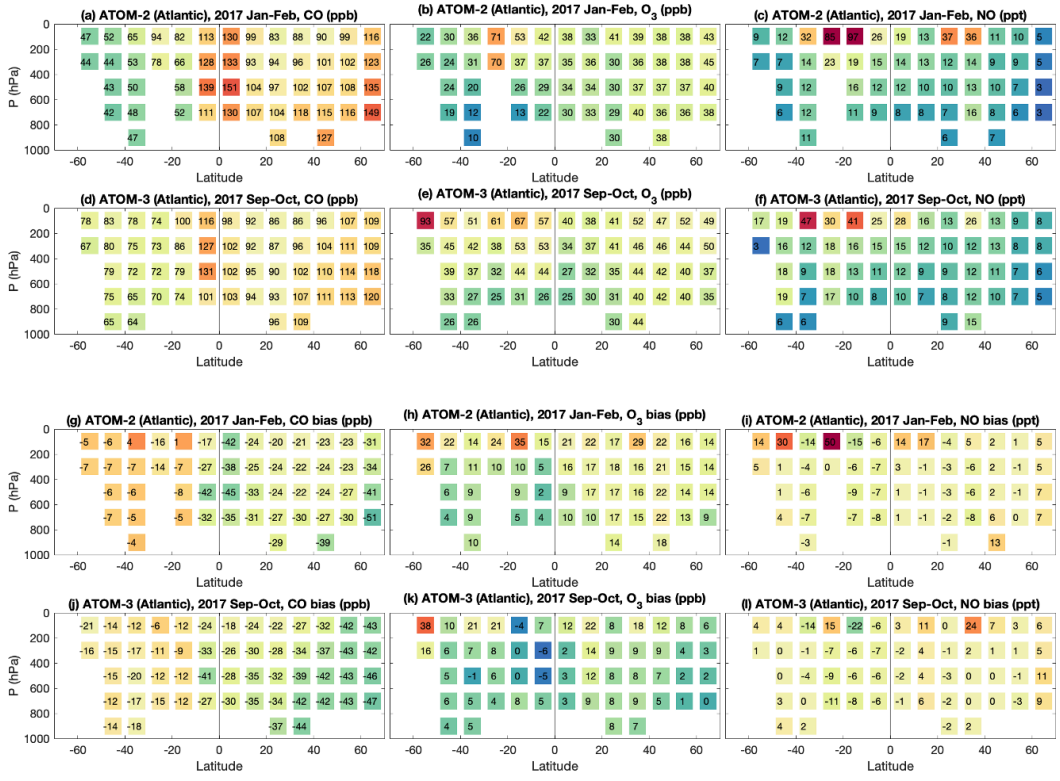

Figure 11. Observations of (a) CO (ppb), (b) O_3 (ppb), and (c) NO (ppt) over Atlantic Ocean during ATom-2 and ATom-3 (d-f). (g-l) corresponding model biases against ATOM observations. The ATom airborne measurements and corresponding MUSICAv0 model results are binned to 10-degree latitude and 200-hPa pressure bins. The values of mean biases for each latitude and pressure bin are labeled in the figure.

https://doi.org/10.5194/gmd-2023-50
Preprint. Discussion started: 4 May 2023
© Author(s) 2023. CC BY 4.0 License.

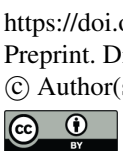

Geoscientific Model Development
Discussions
Open Access
EGU

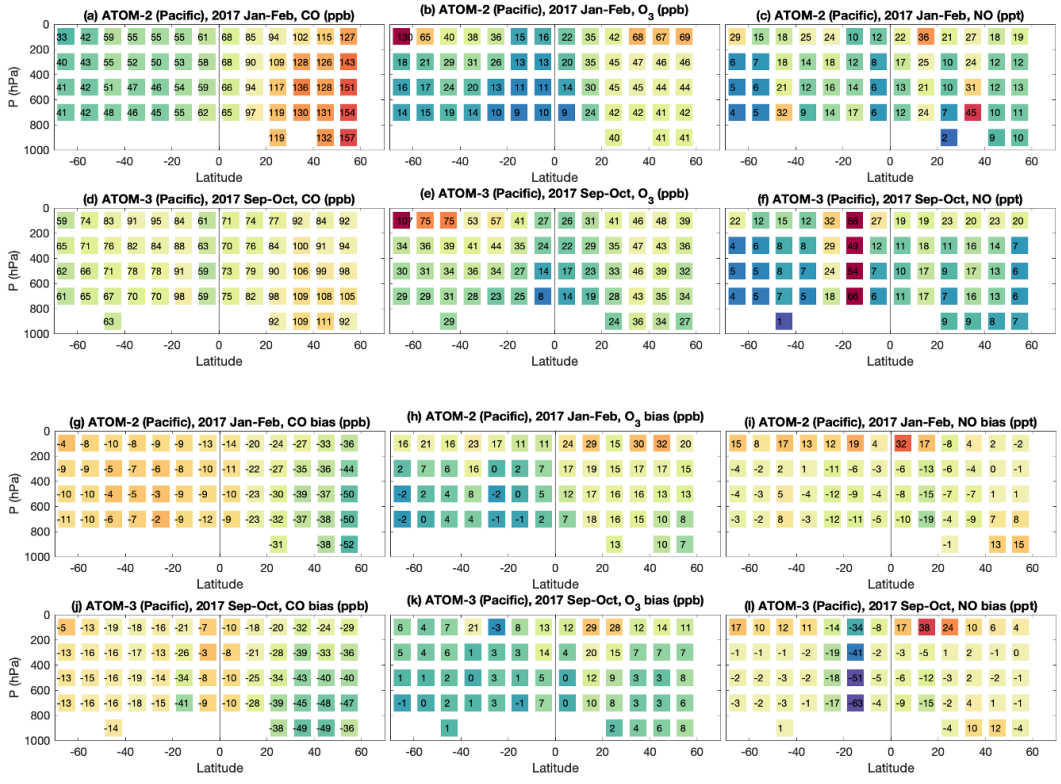

Figure 12. Same as Figure 9 but for over the Pacific Ocean.

https://doi.org/10.5194/gmd-2023-50
Preprint. Discussion started: 4 May 2023
© Author(s) 2023. CC BY 4.0 License.

Geoscientific Model Development Discussions
Open Access
EGU

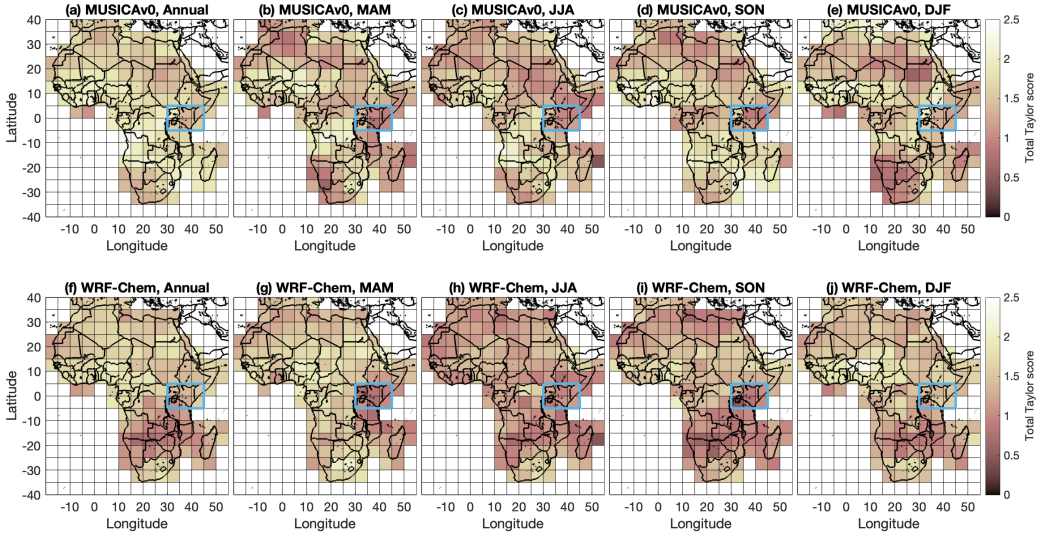

Figure 13. Spatial distribution of total Taylor score of MUSICAv0 and (f-j) WRF-Chem compared to satellite retrievals. In each 5° × 5° (latitude × longitude) pixel, Taylor scores of the model compared to three satellite products (e.g., MOPITT CO column retrievals, OMI tropospheric NO_2 column retrievals, and MODIS AOD) are calculated separately (as shown in Figure S8). Taylor score against each satellite product ranges from 0 to 1. And then three Taylor scores are summed up to obtain the shown total Taylor score (ranges from 0 to 3). Total Taylor score of MUSICAv0 for (a) 2017, (b) MAM (March, April, and May), (c) JJA (June, July, and August), (d) SON (September, October, and November), and (e) DJF (December, January, and February) are shown. The blue box highlights a potential region for future field campaigns and/or in situ observations. (f-j) are similar to (a-e) except for WRF-Chem.

https://doi.org/10.5194/gmd-2023-50
Preprint. Discussion started: 4 May 2023
© Author(s) 2023. CC BY 4.0 License.

Geoscientific Model Development
Discussions
Open Access
EGU

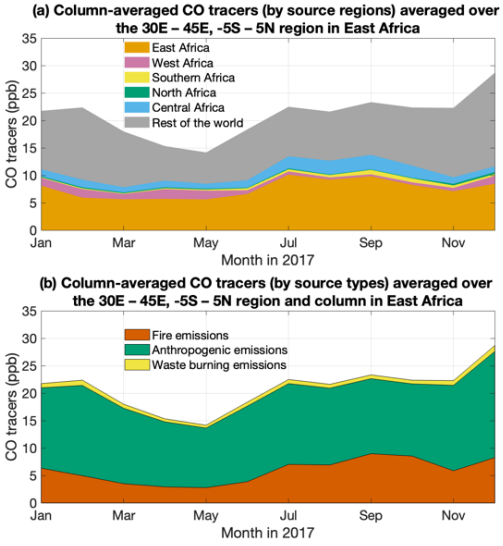

Figure 14. Monthly time series of column-averaged CO tracers in the 30°E – 45°E, -5°S – 5°N region in East Africa. (a) CO tracers of emissions from North Africa (green), West Africa (pink), East Africa (orange), Central Africa (blue), Southern Africa (yellow), and the rest of the world (grey). (b) CO tracers of fire emissions (red), anthropogenic emissions (green), and waste burning emissions (yellow).